Dynamics of Meiotic Sex Chromosome Inactivation and Pachytene Activation in Mice Spermatogenesis

Ábel Vértesy[1,2]; Javier Frias-Aldeguer[1,4]; Zeliha Sahin[1,3]; Nicolas Rivron[1,4]; Alexander van Oudenaarden[1,2] and Niels Geijsen[1,5]

1. Hubrecht Institute-KNAW (Royal Netherlands Academy of Arts and Sciences) and University Medical Center, 3584 CT Utrecht, The Netherlands
2. Department of Genetics, Center for Molecular Medicine, Cancer Genomics Netherlands, University Medical Center Utrecht, The Netherlands
3. Amsterdam UMC, University of Amsterdam, Clinical Genetics, Amsterdam Medical Research, Meibergdreef 9, Amsterdam, Netherlands
4. MERLN Institute for Technology-Inspired Regenerative Medicine, Maastricht University, The Netherlands
5. Faculty of Veterinary Medicine, Clinical Sciences of Companion Animals, Utrecht University, The Netherlands

Abstract

During germ cell development, cells undergo a drastic switch from mitosis to meiosis to form haploid germ cells. Sequencing and computational technologies now allow studying development at the single-cell level. Here we developed a multiplexed trajectory reconstruction to create a high-resolution developmental map of spermatogonia and prophase-I spermatocytes from testes of a Dazl-GFP reporter mouse. We identified three main transitions in the meiotic prophase-I: meiotic entry, the meiotic sex chromosome inactivation (MSCI), and concomitant pachytene activation. We validated the key features of these transitions *in vivo* using single molecule FISH. Focusing on MSCI, we found that 34% of sex chromosomal genes are induced shortly before MSCI, that silencing time is diverse and correlates with specific gene functions. These highlight a previously underappreciated level of regulation of MSCI. Finally, we found that spermatozoal genes in pachytene are activated in a temporal pattern reflecting the future anatomic and functional order of the sperm cell. Altogether we highlighted how precise and sequential changes in gene expression regulate cellular states in meiotic prophase-I.

Introduction

Spermatogenesis is a complex and continuous differentiation process from the spermatogonia to the spermatocyte stages that resolves a switch from mitotic to meiotic divisions to generate haploid sperm cells. This process is accompanied by major morphological, cellular and transcriptional changes, which are not well understood transcriptome-wide nor temporally resolved in a fine manner. Single-cell analysis provided an overall description of spermatogenesis (Chen *et al.*, 2018; Jung *et al.*, 2018; Lukassen *et al.*, 2018) including the analysis of Sertoli cell biology (Green *et al.*, 2018), the comparison of human and mouse spermatogenesis (Hermann *et al.*, 2018) and the analysis of post-meiotic sex chromosome dynamics (Ernst *et al.*, 2019). Here, we developed a multiplex computational approach to finely resolve developmental trajectories of single *Dazl*+ cells over the time of mitotic to meiosis transition.

A male specific feature of meiosis is the incomplete pairing of the X and Y chromosomes during meiosis (termed asynapsis). While in female cells, all chromosomes can form homologous pairs and recombine, in males, the X and Y chromosomes only share a small homologous part, the pseudoautosomal region (PAR). The remaining non-homologous regions stay unpaired, acquire repressive chromatin marks, and eventually form the sex-body within the nucleus (Khalil, Boyar and Driscoll, 2004; van der Heijden *et al.*, 2007). This silencing of the X and Y chromosome during male meiosis is called meiotic sex chromosome inactivation (MSCI) (Henderson, 1963; Turner, 2015). MSCI is thought as a special case of meiotic silencing of unsynapsed chromatin (Shiu *et al.*, 2001) and is an essential step of male meiosis (Royo *et al.*, 2015). While MSCI's post transcriptional regulation, such as H2AX phosphorylation (Mahadevaiah *et al.*, 2001) and ubiquitination (Baarends *et al.*, 2005) are well described, the transcriptional control of these regulators and the dynamics of gene expression silencing are still to be identified.

Another feature of male meiosis is a massive wave of gene expression at the pachytene stage (Fallahi *et al.*, 2010), when mid-meiosis cells express a remarkable array of post-meiotic genes involved in spermiogenesis (da Cruz *et al.*, 2016). The dynamics of the activation of this transcriptional program, and whether sex chromosomal genes can escape MSCI are open questions in the field, which we analyzed in detail.

We thus set out to draw a temporally resolved, transcriptome-wide gene expression atlas from meiotic commitment until prophase-I, in order to unravel transcriptional changes that coordinate germ cell differentiation and meiotic transition. We sequenced mRNA from

1880 single cells, multiplex reconstructed their temporal order *in silico*, which we validated *via* microscopy. This allowed us to describe the precise sequence of transcriptome-wide changes upon MSCI and pachytene activation.

Results

1. Single-cell transcriptomics of *Dazl*+ germ cells identifies stem cells along with 4 stages of prophase-I

Dazl is expressed from spermatogonial to early pachytene stage (Kim, Cooke and Rhee, 2012). We thus used *Dazl-GFP* reporter mice (Chen *et al.*, 2014) to isolate cells during meiotic entry and prophase from testes of adult mice (2-4 month) (Fig. 1A). We applied single-cell mRNA sequencing using the SORT-seq protocol (Muraro *et al.*, 2016), and sequenced 1880 single cells from 3 mice. After trimming and sequence alignment to the mm10 reference transcriptome (Online Methods), we filtered low quality cells with fewer than 3000 unique (UMI corrected) transcripts and selected 1274 high-quality germ cells. These were normalized to the median transcript count (20488 per cell), allowing us to compare the relative expression across cells (Fig. S1A, Online Methods).

To determine whether transcriptional changes are continuous or rather separated into discrete steps, we classified cells by transcriptome-wide, unsupervised k-medoids clustering on Spearman correlation coefficients. Cells were clustered in 5 groups (Fig. 1 B, C) based on all genes with at least 10 transcripts in minimum 50 cells. Importantly, we did not predefine the number of expected stages, but estimated it based on the within-cluster-dispersion of data points (Grün *et al.*, 2016). The established clusters are also supported by saturating gap statistics, a positive cluster silhouette. High Jaccard indices across bootstrapping rounds indicate that the clusters are reproducible (Fig. S1 C-E, Online Methods). These clusters are not influenced by animal-to-animal variation, batch variation nor library complexity (Fig. S2). After we ruled out batch effects, we excluded contamination from somatic cells based on a lack of expression of Sertoli or Leydig cell specific markers *Stra6* and *Amh* (Fig. 1D) (O'Shaughnessy, Morris and Baker, 2008; Griswold, 2016). On the contrary, cells showed a high expression of *Dazl*, and of the meiotic prophase marker *Sycp3* (Fig. 1D).

Cells forming cluster 1 express markers of differentiating spermatogonia, like *Dmrt1* (Matson *et al.*, 2010), *Kit* (Yoshinaga *et al.*, 1991), and earlier progenitor markers, as

Lin28a (Chakraborty *et al.*, 2014) (Fig. 1 D). Cells forming the cluster 2 uniquely express *Stra8*, the key gene marking meiotic entry (Anderson *et al.*, 2008). Cells forming cluster 3 specifically upregulate the zygotene specific Cyclin B3 (*Ccnb3*) (Nguyen *et al.*, 2002), which is located on the X chromosome, and marks the last stage with sex chromosomal expression (zygotene I). Cells forming cluster 4 upregulated H2A histone family member X (*H2afx*), the histone variant associated with meiotic sex chromosome inactivation (MSCI) in early pachytene. Finally, cells forming cluster 5 specifically express the pachytene marker lactate dehydrogenase C (*Ldhc*), a testis-specific enzyme in anaerobic glycolysis (Goldberg *et al.*, 2010). Taken together, we concluded that *Dazl*+ cells represent 5 transcriptionally distinct subpopulations with clear transcriptional signatures.

2. Identified clusters correspond to subsequent stages of prophase-I

To better characterize the established clusters, we compared their gene expression by differential gene expression analysis (Table S1-S2, Data S2). Cluster 1 on the left edge of the t-SNE map (Fig 1B) encloses ~33% of the cells (Fig. S2A). They are uniquely expressing *Dmrt1* and other markers of mitotically dividing cells including *Ccnd1, Cenpa, Mcm2*, *Ccdc6, Gsr, Ccdc6 and Crabp1 (*Data S2, Table S1*)*. While most spermatogonial cells are *Kit*+, we noticed that some markers of the undifferentiated state, including *Uchl1* or *Lin28a* (Luo, Megee and Dobrinski, 2009; Griswold, 2016) are partially co-expressed with Kit+ cells (Data S1).

On the right side of the t-SNE map (Fig 1B), 36% of the cells form Cluster 5 (Fig. S2A). These cells are characterized by a high expression of pachytene markers such as the *Adam* genes, *Ldha, Ldhc, Crisp2, Ybx* genes, *Meig1* and *Piwil1* (Jan *et al.*, 2017) (Data S2), consistent with early expression of post-meiotic genes (da Cruz *et al.*, 2016).

These two opposite clusters (1 and 5) are defined by many uniquely expressed genes within our dataset (Table S1-S2). Between these, we found 3 intermediate clusters with fewer specific genes. These clusters therefore are largely determined by unique combinations of up- and downregulated genes. For example, we found that Cluster 2 uniquely expresses *Stra8* and *Prdm9* suggestive of differentiated spermatogonial or preleptotene stage (Sun *et al.*, 2015). At the same time, they also started to upregulate the meiotic *Sycp* genes (Margolin *et al.*, 2014).

The meiotic entry is accompanied by a global transcriptional silencing (Monesi, 1965; Ernst *et al.*, 2019). Indeed, we observed that the meiotic entry (Cluster 2) corresponds to

129 a transient drop in raw transcript counts in clusters 2-4 (Fig. 2D), which is not explained
130 by differences in sequencing depth (Fig. S1F). Despite this drastic silencing, each cluster
131 (1 & 2) showed the upregulation of a specific subset of genes, as compared to the earlier
132 stage (Table S2).

133 The next two clusters (3 & 4) displayed the peak expression of *Dazl*, *Sycp1* & 3. They also
134 a shared expression of zygotene specific genes involved in recombination, such as
135 *Hormad1* (Shin *et al.*, 2010) and *Meiob* (Luo *et al.*, 2013), as well as *Elavl3*, *Gml* and *Mnd1*
136 (Data S2). A key difference is that while cluster 3 shows high expression for many sex
137 chromosomal genes (e.g. *Scml2*, *Fmr1*), cells in clusters 4 and 5 only express residual
138 amounts of these mRNAs.

139 Taken together we concluded that clusters 1 to 5 show unique gene expression patterns,
140 which recapitulated established stages of prophase-I. We built an online explorer for all
141 genes (https://vertesy.shinyapps.io/ExpressionBrowser/) and listed all differentially
142 expressed genes (Table S1-2). We also found subpopulations within these clusters,
143 suggesting finer transitions. To analyze these systematically, we extended our
144 computational analysis to a staging-free approach, better reflecting the continuity of
145 spermatogenesis.

146 3. Multiplex trajectory reconstruction precisely recapitulates established 147 meiotic events

148 Multiple recent approaches successfully reconstructed pseudotemporal trajectories from
149 single-cell transcriptomes using either principal curves (Petropoulos *et al.*, 2016), TSCAN
150 (Ji and Ji, 2016), or Monocle 2 (Qiu *et al.*, 2017). We reconstructed temporal order in our
151 data set by all three methods (Fig. S3). It resulted in a similar, but not identical ordering
152 (min. pairwise $r > 0.95$) (Fig. 2A, Online Methods). From the three reconstructions we
153 calculated the consensus trajectory reflecting developmental time (Fig. 2B), which allowed
154 us to analyze transcriptome dynamics in a more reliable and precise way than possible
155 before.
156

157 First of all, this map recapitulated the previously determined stages, while revealing much
158 finer events, as detailed below (Fig. 2E). We then used *in vivo* samples to validate this
159 reconstruction, by 3-color single-molecule RNA fluorescence in situ hybridization
160 (smFISH). We selected the (pre)leptotene gene *Stra8* (cluster 2) (Anderson *et al.*, 2008),

161 the pachytene specific *H2afx* (cluster 4) and the gene *Actb*, which is primarily expressed
162 in spermatids (Ventela *et al.*, 2000). The smFISH clearly pinpointed spatially-separated
163 populations. Cells formed a sparse outer layer of *Stra8*+ (pre)leptotene cells decorating a
164 dense intermediate layer of *H2afx*+ pachytene cells, enclosing an inner ring of *Actb*+
165 spermatid cells (Fig. 2C). Additionally, the three key transcriptional events (silencing at
166 meiotic entry, meiotic sex chromosome inactivation and pachytene activation) are
167 correctly recapitulated (Fig. 2D).

168 We then focused on finer differences. The reconstruction precisely predicted that *Lin28a*
169 is expressed only in the earliest stage spermatogonia (Chakraborty *et al.*, 2014). It also
170 accurately predicted that *Stra8* peaked shortly before *Prdm9* (Sun *et al.*, 2015).
171 Remarkably, all other analyzed marker genes also peaked in the expected developmental
172 order (Fig. 2E). Altogether, we concluded that the consensus trajectory faithfully
173 recapitulated the developmental progress of early spermatogenesis, thus, it allows for a
174 reliable, in-depth computational analysis of gene expression patterns.
175

176 4. Temporal expression maps show continuous differentiation from 177 (pre)leptotene to pachytene

178 Next, we analyzed all genes' expression profiles along the trajectory. First, we classified
179 gene expression dynamics, and found that most genes showed a single expression peak
180 (Fig. 3A). We then analyzed the co-expression profiles of genes peaking around
181 (pre)leptotene. This showed how the meiotic master regulator *Stra8* expression preceded
182 other preleptotene genes. As an example, we highlighted the cascade of *Stra8, Tex15*
183 and *Dmc1* activation within one stage (Fig. 3B, selected by highest z-score).

184 To understand this sequential activation deeper, we selected genes with a single
185 expression maximum along the trajectory (Online Methods, Fig. S4). We then ordered
186 these genes by time of peaking (Fig. 3C). First, it showed the three most unique stages in
187 our dataset: spermatogonia, (pre)leptotene and pachytene. By showing the number of
188 genes changing at each stage, it also highlighted the magnitude of changes upon meiotic
189 entry, and pachytene activation. The analysis also suggests that sequential and sharply
190 timed gene activation might be the regulatory clockwork of spermatogenesis, possibly
191 triggering genes with wider expression profiles as seen in (Fig. 3A, B).

192 This analysis allowed us to identify genes co-expressed with known marker genes, which
193 in turn can help to characterize their function. As an example, we identified 21 genes (r >
194 0.9) with expression patterns similar to *H2afx* (Fig. 3D). The best correlating genes were
195 Hemt1 (Gml2) and *Gml* (*Hemt3*) (Fig. 3E), a pair of uncharacterized genes, although *Gml*
196 was previously identified in prophase spermatocytes (Xue *et al.*, 1999).

197 To validate this stunning co-expression of *Hemt1* and *H2afx*, we performed smFISH (Fig.
198 3F-G). This confirmed their co-expression within a spatially-restricted population, which
199 suggests a co-functionality. To help researchers finding other co-expressed genes, we
200 implemented an interactive co-expression browser as part of our online toolbox. Taken
201 together, we created a compendium of gene expression dynamics in meiotic prophase-I
202 and developed interactive tools for further investigation.

203 5. Silencing of an *n-Myc* transcription factor network coincides with global 204 silencing during meiotic entry

205 Previous studies elegantly inferred transcription factor binding sites for large clusters of
206 cells (Green *et al.*, 2018) or clusters genes (Jung *et al.*, 2018) during meiotic entry.
207 Building upon this, we aimed at understanding the transcriptional programs behind the
208 global silencing during meiotic entry. Therefore, we compared the transcriptome of
209 spermatogonial and (pre)leptotene cells (Fig. 4A, Table S3). We analyzed these by
210 identifying significantly enriched GO-terms of >4-fold differentially expressed genes
211 (Online Methods, Table S3). The GO-terms were then clustered according to semantic
212 similarity (Supek *et al.*, 2011).

213 Besides the clear and expected switch from mitotic to meiotic program, the transcriptome
214 of (pre)leptotene cells showed strong metabolic silencing (Fig. 4B, C). Metabolic silencing
215 also may explain the drastic decrease of mRNA content in late spermatogonia, which lasts
216 until pachytene (Fig. 2D). Many housekeeping genes were silenced, and their expression
217 generally varied throughout the entire prophase-I (Data S3).

218 To better understand how meiotic entry is regulated, we focused on transcription factors.
219 As many transcription factors are expressed at the detection limit of single-cell
220 sequencing, they often cannot be reliably identified by differential gene expression
221 analysis. Therefore, we analyzed the transcription factor binding site enrichment in the
222 promoters of differentially expressed genes (Online Methods) (Matys, 2006; Portales-
223 Casamar *et al.*, 2010; Kuleshov *et al.*, 2016). To gain statistical power, we analyzed >2-

224 fold enriched genes in either cluster (Fig. 4D, enriched GO-terms recapitulated previous
225 results, see Table S3).

226 Eight transcription factors showed highly significant (p.adj. <0.01) binding site enrichment
227 in the spermatogonial genes (Fig. 4E). In contrast, no transcription factor was unique to
228 the (pre)leptotene stage, while some (*Sp1* and *Smad4*) showed a highly significant
229 enrichment in both gene sets (Table S3).

230 We found that six out of eight of the predicted transcription factors from a tightly
231 interconnected hub (Fig. 4F, Online Methods) based on protein interaction network
232 (Szklarczyk *et al.*, 2017). This pinpoints a core regulatory network may regulate the
233 mitotic-meiotic transition. When testing these predictions on our data, we found that most
234 predicted spermatogonia-specific factors (*n-Myc, Trp53, Egr1, Smad4*) are silenced
235 expectedly. Curiously *Sp1* –which cooperates with *Smad4* in TGF-β signaling– showed
236 the opposite trend (Feng, Lin and Derynck, 2000). *Nrf1* (Wang *et al.*, 2017) was expressed
237 continuously, while *Myb* and *Elk1* were not detected (Fig. 4G).

238 Taken together, explicit silencing -rather than activation- drives the transcriptional switch
239 in meiotic entry. The silencing showed a particularly strong metabolic control. *Myc* is
240 known to regulate more than 11% of all genes, in particular metabolic ones (Fernandez,
241 2003). Hence, the downregulation of the spermatogonia -specific *n-Myc* variant (Braydich-
242 Stolle et al., 2007) may explain the global transcriptional silencing upon meiotic entry.

243 6. 34% of the sex chromosome genes are induced right before sequential 244 inactivation by MSCI.

245 The second major wave of transcriptional silencing in prophase-I is the meiotic sex
246 chromosome inactivation (MSCI). This leads to the global silencing of the sex
247 chromosomes (Henderson, 1963; McKee and Handel, 1993). While post-meiotic silencing
248 has been analyzed in detail (Ernst *et al.*, 2019), and multiple recent single-cell studies
249 referred to MSCI (Chen *et al.*, 2018; Jung *et al.*, 2018; Lukassen *et al.*, 2018). However,
250 the patterns of gene silencing during MSCI, and the underlying regulation remained open
251 questions.

252 To tackle this question, we classified all sex chromosomal genes along the trajectory. This
253 confirmed their silencing at late zygotene, but also showed considerable gene-to-gene
254 variability in silencing dynamics (Fig. 5A). Four sets of these genes formed distinct waves
255 of transcription. The largest wave contains genes expressed in spermatogonia (cluster 1).

This, in turn, is consistent with the observations that the X chromosome is enriched in premeiotic genes (Khil *et al.*, 2004; Koslowski *et al.*, 2006). Yet, interestingly, many other genes were transiently induced prior to MSCI. The combination of these patterns (gradual silencing & pre-MSCI transcriptional burst) also clarifies why the total expression from both the sex chromosomes ramps up before MSCI (Fig. 5B). We also confirmed our observation using a recently published dataset (Ernst *et al.*, 2019).

We also noticed that the sex chromosomal expression clearly anti-correlated with the expression of *H2afx* (Fig. 5B, stages marked by a color bar on top). This observation contrasts with the ubiquitous deposition of *H2afx* along the genome, and with the idea that is mostly regulated post-transcriptionally (Turner *et al.*, 2004; Bellani *et al.*, 2005; Turinetto and Giachino, 2015). *H2afx* can be phosphorylated by *Atm, Atr* and *Pkrdc,* and we confirmed that only *Atr* is expressed during MSCI (Bellani *et al.*, 2005), however it shows decreasing mRNA levels (Fig. 5C). The lack *Atr* induction around MSCI alongside the observation that *H2afx* is induced precisely at this time suggests that the timing of MSCI is partly controlled by *H2afx* transcription. Possibly, then the main role of the *Atr* could be to activate the newly deposited histones.

It has been proposed that MSCI is simply a selective lack of reactivation of the sex chromosomes during pachytene (Page et al. 2012). Here, we show that MSCI is an separate silencing event (Fig. 5B). First of all, sex chromosomal transcription sharply falls before pachytene activation. Second, many sex chromosomal genes were specifically upregulated before silenced (Fig. 5A). Finally, transcript levels after (pre)leptotene silencing are stable until pachytene, except from the sex chromosomes (Fig. 2D).

Some X chromosomal genes have autosomal paralogs, which switch expression to the autosomal copy upon MSCI. We indeed see the timing and extent of autosomal compensation in our data. As examples, we detected that when the X chromosomal gene *Rpl10* is silenced by MSCI, its paralog, *Rpl10L* on chr12 is induced (Jiang *et al.*, 2017). The paralog pairs *Pgk1* (chrX) - *Pgk2* (chr17), and the *Cetn2* (chrX) - *Cetn1* (chr18) (Hart *et al.*, 1999) show the same trend (Data S6).

It is unknown whether MSCI follows any pattern and if genes are silenced in any particular order. The best-studied example of chromosome-wide silencing is the X chromosome inactivation (XCI) in female mice. Although XCI evolved to achieve dosage compensation, both involve the silencing of the whole X chromosome. Silencing in XCI is primarily

288 governed by chromosome structure and proximity to the X-inactivation center (Nora *et al.*,
289 2012; Engreitz *et al.*, 2013).

290 We therefore tested the possibility of a silencing center, or a silencing bias towards either
291 chromosomal end. In the telocentric chromosomes of mice, centromeres occupy one end
292 of each chromosome. For the X and Y chromosomes, the other end forms the
293 pseudoautosomal region (PAR). While the centromere holds the sister chromatids
294 together, the PAR holds the X & Y chromosomes together in meiosis. Thus, both ends
295 might bias chromatin silencing.

296 We then analyzed the silencing dynamics along the X chromosome, on a linear basis.
297 While we found ample variability in silencing dynamics, we detected no spatial effect
298 towards either end of the X chromosome, nor towards the *Xist* locus (Data S4). Thus, we
299 concluded that unlike X-inactivation, MSCI is unlikely to be governed by proximity to an
300 inactivation center.

301 Genes in the pseudoautosomal regions (PAR) are X/Y homologous, and not silenced, so
302 they could be used as an internal negative control for MSCI. In mice however, PAR only
303 contains 3 active genes (Kasahara et al., 2010). While *Sts*, and *Asmt* (*Hiomt*) transcripts
304 were not detected, *Mid1* (*Fxy*) indeed showed low, but constant raw transcript counts
305 throughout prophase-I (Fig. S6E).

306 We further examined the expression of the latest silenced genes in the second half of
307 MSCI (cluster 4). We found a small set of genes with remarkably high expression (Fig.
308 5D). These genes –except *Prdx4*– were specifically induced in zygotene and showed high
309 expression, when the expression of other sex chromosomal genes was already
310 decreasing (Fig. 5E). *Scml2* is a testis-specific polycomb protein, which regulates the
311 ubiquitination state of *H2afx*. It showed one of the strongest and latest expression peak,
312 underlining its important role in controlling MSCI (Luo *et al.*, 2015) and genes escaping
313 silencing (Adams et al. 2018).

314 Based on the functional cues among the late-silenced genes, we performed a
315 comprehensive analysis of gene function during silencing. We classified sex chromosomal
316 genes into fast- and slow-silenced categories based on their characteristic silencing time
317 (Online Methods). For each group, we calculated GO-term enrichment as compared to all
318 sex chromosomal genes (Online Methods). We found that while early-silenced genes
319 were typically localized to the nucleus (43% of the genes, FDR < $4e^{-3}$). Inversely, late-
320 silenced genes were preferentially localized to the cytoplasm (56%, FDR < $2e^{-6}$) and were

enriched in genes encoding mitochondrial proteins (19%, FDR < $2e^{-5}$). This further supported the notion that silencing is a coordinated process starting with regulatory genes and followed by cytoplasmic and metabolic genes (catalytic activity: 34% of late genes, FDR < $8e^{-3}$) (Table S4).

7. *Slitrk2* and other genes escape MSCI

We also noticed that the *Ndufa1* (Fig. 5D), is not only the last gene to be downregulated, but it also maintains a steady absolute transcript level throughout pachytene, possibly by escaping inactivation. Whether genes escape MSCI is debated in recent literature (Chen *et al.*, 2018; Jung *et al.*, 2018). Transcripts detected in pachytene can either be due to mRNA preservation over several days, or due to an active transcription from MSCI. Therefore, it is important to characterize if such genes show increased expression after MSCI, and to validate their expression pattern independently.

To examine if other sex chromosomal genes are also detected after MSCI, we calculated the average raw transcript counts in cluster 5 (as normalized counts may be misleading, see Fig. 2D and Online Methods). We identified 27 genes on chromosome X with above and an average of one transcript per cell (Fig. 5G). This correspond to approximately 10-100 transcripts per cell, given the estimated sensitivity of single-cell methods (Grün, Kester and van Oudenaarden, 2014). Importantly, we detected more transcripts for these 27 genes after MSCI, suggesting that their expression is not simply due to mRNA preservation.

Slitrk2 showed the most striking expression pattern, as it was specifically upregulated after MSCI (Fig. 5G). *Slitrk2* is the only gene expressed from the hybrid sterility locus (*Hstx1/2*). It has been described to escape silencing in *domesticus X musculus* hybrids (Bhattacharyya *et al.*, 2014). It is not expressed in Sertoli cells (Zimmermann *et al.*, 2015), and we validated its expression *in vivo* by smFISH (Fig. 5J-K).

Mapping these 27 escapee genes on the X chromosome showed a clustered pattern around the *Zfx*, *Irak1*, and *Xist* loci (Fig. 5H). Note, that *Xist* itself is not expressed in males. ATAC-seq has previously identified the *Xist* locus as one of the most open chromatin regions during XCI in females (Giorgetti *et al.*, 2016), which may contribute to the lack of silencing in genes located in proximity of *Xist*. In addition, we noticed that many of the escaping genes from the *Xist* locus are long, and often non-coding genes. Indeed,

352 the transcript length of the 27 escapee genes are significantly longer than other X
353 chromosomal genes (one-sided MWW test, $p<0.006$).

354 When compared to known escapees in post-meiotic sex chromosome inactivation
355 (Namekawa *et al.*, 2006) and MSCI, only *Mageb.ps-1* is shared. Similarly, when compared
356 38 XCI escapees (Berletch *et al.*, 2015) with MSCI, only *Car5b* was common (Fig. 5I).
357 These observations suggest that a mechanism of silencing and escaping distinct from
358 previously studied cases (e.g. XCI) occurs during the meiotic phase.

359 Finally, we wanted to know if escapee genes show specific expression dynamics during
360 prophase. Therefore, we clustered gene expression profiles along the trajectory. We found
361 that most genes follow a pattern similar to *Ndufa1*, while the expression pattern of *Slitrk2*
362 is unique (Fig. S5A). Yet, both patterns appeared as residual rather than functional. This
363 is because relative transcript counts –within the expanding pachytene transcriptome–
364 remained in all cases low. Escape from silencing then might simply be the consequence
365 of open chromatin amidst global transcription. An exception to this might be Slitrk2.

366 Taken together, we found that a third of sex chromosomal genes are specifically induced
367 before silencing by MSCI. Although MSCI is a short event in meiosis, we found remarkable
368 differences in the silencing time of genes. While broad chromosome structure does not
369 appear to affect silencing time, we found functional cues. early-silenced genes are mostly
370 nuclear, but late-silenced genes are often cytoplasmic or mitochondrial. This leads to the
371 interesting possibility of a “regulation first, processing second” silencing pattern. Yet, to
372 understand the role of MSCI, one must consider a combination of ancestral and newly
373 acquired functions (Turner *et al.*, 2004). MSCI might have evolved for one reason, *e.g.*
374 global silencing of unsynapsed chromatin, and once in place, it could evolve to new
375 regulatory functions.

376

377 8. Genes in pachytene are activated in the functional order of mature sperm 378 anatomy.

379 The transient silencing during leptotene and zygotene ends before pachytene (Monesi,
380 1965). This leads up to 9-times more cellular mRNA than in earlier stages (Fig. 2D, inset,
381 at 900 on the trajectory). In accord with a global transcriptional activation, cells in
382 pachytene reach the most diverse transcriptome in our dataset, as quantified by entropy
383 (Fig. S4E).

384 To characterize this massive transcriptional wave, we first identified genes upregulated in
385 pachytene by differential gene expression analysis (Fig. 6A). We selected all genes that
386 showed a 3-fold upregulation compared to all other cells (Online Methods). We classified
387 these into 3 categories by k-means clustering of z-score normalized rolling average
388 expression profiles (Fig. 6D). Clusters showed reproducibility >98% over 10000
389 bootstrapping rounds, and gene classes displayed sharp, distinct activation profiles (Fig.
390 6B & E).

391 Many immediate genes had functions linked to the pachytene transcriptional activation
392 itself. Other immediate genes encoded proteins for energy production (e.g. The
393 mitochondrial cytochrome c oxidase genes) (Fig. 6C). Piwi-pathway related genes formed
394 the next wave in the 'intermediate class of genes (*Piwil1*, *Tdrd1*, *Pld6* and *Gtsf1*),
395 protecting against transposons (Aravin, Hannon and Brennecke, 2007).

396 Yet, most genes activated in pachytene have post-meiotic roles (Da Cruz, 2016). Many of
397 the enriched functions are first relevant in elongating spermatid (e.g. flagella formation) or
398 in mature spermatozoa (e.g. binding to zona pellucida). These genes are thus surprisingly
399 transcribed more than a week before their utilization. The *Adam* gene family (Primakoff
400 and Myles, 2000) is a typical example of the pachytene-activated, fertilization-related
401 genes. One of these gradual genes is *Adam32* (Fig. 6F). We validated its expression by
402 smFISH (Fig. 6I), which also matched the expression pattern found in neonatal testis (Choi
403 *et al.*, 2003).

404 We also found distinct functional signature of immediate and gradual genes, while the
405 intermediate class of genes showed a blend of functional enrichments (Fig. 6G).
406 Interestingly, the genes were activated in parallel order to the order they will be used in
407 the mature spermatozoa. While immediate genes play a role in flagella formation and cell
408 movement, late genes are involved in fertilization (Table. S6). Accordingly, enriched GO-
409 terms in the immediate and gradual classes mapped to different anatomical regions of the
410 spermatozoa (Fig. 6H).

411 Surprisingly, while these genes are transcribed in a precise order, they are only translated
412 and used more than a week later. This temporal discrepancy highlights the important role
413 of mRNA storage in spermatogenesis. In accord, we noted that pachytene activation is
414 exactly the time when *Dazl*, an RNA binding protein, is downregulated (Fig. 1D).
415 Altogether, we observed a sequential pattern of gene activation in pachytene cells that

416 reflect the spatial anatomy of the mature sperm. This temporal pattern might show a
417 spatial pattern of maturation of the germ cell, from the tail to the head.

418 Discussion

419 Currently, meiotic entry in mammals is not well understood, as highlighted by our inability
420 to induce meiosis purely *in vitro*, without the co-culture of explanted tissues. To gain a
421 transcriptome-wide and time-resolved insight, multiple recent studies applied single-cell
422 mRNA sequencing combined with pseudo-temporal reconstruction (Chen *et al.*, 2018;
423 Green *et al.*, 2018; Hermann *et al.*, 2018; Jung *et al.*, 2018; Lukassen *et al.*, 2018; Ernst
424 *et al.*, 2019). These studies provided excellent resources and greatly contributed to
425 understand the whole span of spermatogenesis. Yet, additional questions require deeper,
426 fine-tuned, computational analysis.

427 Our study focused on early meiosis up until pachytene. We found that in contrast with the
428 multitude of morphological stages, there are only three major transcriptomic events. In the
429 first major transition spermatogonia committed to meiosis. This is accompanied by a
430 global shrinkage of the transcriptome and a clear functional switch. Cells shift from a
431 mitotic and catabolic to a meiotic and recombination-related transcriptome. This functional
432 switch however appears to be regulated by a one-sided silencing of a transcription factors
433 hub around *n-Myc*, while no comparable network is upregulated.

434 The second major transition is meiotic sex chromosome inactivation. It is thought that the
435 phosphorylation of the silencing histone variant *H2afx* controls the timing of inactivation.
436 We however found that *H2afx* gene is induced exactly during MSCI and it is anti-correlated
437 to sex chromosomal expression. These together suggest that the timing of MSCI is
438 controlled by the surplus of *H2afx* expression. At the same time *Atr* expression is flat,
439 which may hint towards no temporal control on the post transcriptional level.

440 We then characterized chromosome-wide activation and silencing patterns before, and
441 during MSCI. We found that sex chromosomal genes are silenced at distinct times,
442 challenging established models for MSCI. For example, if repression would only appear
443 to protect DNA, we would not expect that genes silence in a coordinated, sequential
444 manner.

445 In general, silencing follows two major patterns: gradual silencing and transient activation
446 followed by silencing. We found that 34% of sex chromosomal genes were specifically

447 induced before MSCI. We speculate that some of these gene products may serve as buffer
448 or pool until autosomal genes take over their functions in pachytene. Additionally, many
449 of these transiently activated genes were involved in regulating gene expression.
450 Interestingly, the chromatin regulator *Scml2* (Hasegawa *et al.*, 2015; Luo *et al.*, 2015;
451 Adams *et al.*, 2018) is one of the genes strongest induced before, and latest silenced upon
452 MSCI, highlighting that gene function and silencing time are concerted. In addition, genes
453 activated just before MSCI might act as a trigger for the third major transition, the
454 pachytene activation.

455 Taken together, sex chromosomes are silenced in a functional, rather than structural
456 order, raising the possibility that MSCI is involved in gene regulation. This, in turn, could
457 also explain why MSCI is essential for meiotic program. Nevertheless, we think there is
458 no single purpose behind MSCI: gene regulation could have evolved atop of its ancestral
459 functions. To deeper understand MSCI, one could complement chromatin profiling with
460 single-cell mRNA-seq, as for PMSCI (Ernst *et al.*, 2019), or perform single-cell chromatin
461 accessibility profiling.

462 Finally, the third major transition in prophase-I is pachytene activation. This global
463 transcriptional activation boosts cellular mRNA content up to 9-fold. We found that
464 immediately and gradually activated genes are functionally distinct. While immediate
465 genes were related to energy metabolism and spermatozoal movement, gradual genes
466 were related to fertilization. Accordingly, the corresponding gene products mapped
467 exclusively to the posterior, or anterior parts of the mature sperm.

468 In sum, we elucidated key events in of early meiosis, and provided a transcriptome-wide,
469 precisely timed, gene expression atlas for online exploration. Our approach hopefully will
470 be followed by functional studies showing the importance of timing in meiosis.

471 Acknowledgements

472 We would like to thank Mauro help for experimental help, Willy Baarends and Joost
473 Gribnau for valuable comments on the manuscript, and help with histological analysis,
474 Stefan van der Elst and Reinier van der Linden for help with FACS sorting, Nicolas Battich
475 for advices on microscopy analysis, Josi Peterson-Maduro for logistic help and Fanny
476 Sage for the mouse drawing.

477

References

Adams, S. R. *et al.* (2018) 'RNF8 and SCML2 cooperate to regulate ubiquitination and H3K27 acetylation for escape gene activation on the sex chromosomes', *PLoS Genetics*, 14(2). doi: 10.1371/journal.pgen.1007233.

Anders, S. and Huber, W. (2010) 'Differential expression analysis for sequence count data', *Genome biology*, 11(R106), pp. 1–12. doi: 10.1186/gb-2010-11-10-r106.

Anderson, E. L. *et al.* (2008) 'Stra8 and its inducer, retinoic acid, regulate meiotic initiation in both spermatogenesis and oogenesis in mice', *Proceedings of the National Academy of Sciences*, 105(39), pp. 14976–14980. doi: 10.1073/pnas.0807297105.

Aravin, A. a, Hannon, G. J. and Brennecke, J. (2007) 'The Piwi-piRNA pathway provides an adaptive defense in the transposon arms race.', *Science (New York, N.Y.)*, 318(5851), pp. 761–4. doi: 10.1126/science.1146484.

Baarends, W. M. *et al.* (2005) 'Silencing of unpaired chromatin and histone H2A ubiquitination in mammalian meiosis.', *Molecular and cellular biology*, 25(3), pp. 1041–53. doi: 10.1128/MCB.25.3.1041-1053.2005.

Bellani, M. A. *et al.* (2005) 'SPO11 is required for sex-body formation, and Spo11 heterozygosity rescues the prophase arrest of Atm-/- spermatocytes.', *Journal of cell science*, 118(Pt 15), pp. 3233–45. doi: 10.1242/jcs.02466.

Bengtsson, M. *et al.* (2005) 'Gene expression profiling in single cells from the pancreatic islets of Langerhans reveals lognormal distribution of mRNA levels', *Genome research*, pp. 1388–1392. doi: 10.1101/gr.3820805.4.

Berletch, J. B. *et al.* (2015) 'Escape from X inactivation varies in mouse tissues.', *PLoS genetics*. Edited by M. S. Bartolomei, 11(3), p. e1005079. doi: 10.1371/journal.pgen.1005079.

Bhattacharyya, T. *et al.* (2014) 'X Chromosome Control of Meiotic Chromosome Synapsis in Mouse Inter-Subspecific Hybrids', *PLoS Genetics*. Edited by B. A. Payseur, 10(2), p. e1004088. doi: 10.1371/journal.pgen.1004088.

Binns, D. *et al.* (2009) 'QuickGO: a web-based tool for Gene Ontology searching', *Bioinformatics*. Oxford University Press, 25(22), pp. 3045–3046. doi: 10.1093/bioinformatics/btp536.

Braydich-Stolle, L. *et al.* (2007) 'Role of Src family kinases and N-Myc in spermatogonial stem cell proliferation', *Developmental Biology*, 304(1), pp. 34–45. doi: 10.1016/j.ydbio.2006.12.013.

Van Den Brink, S. C. *et al.* (2017) 'Single-cell sequencing reveals dissociation-induced gene expression in tissue subpopulations', *Nature Methods*, 14(10). doi: 10.1038/nmeth.4437.

Cannoodt, R., Saelens, W. and Saeys, Y. (2016) 'Computational methods for trajectory inference from single-cell transcriptomics', *European Journal of Immunology*, 46(11), pp. 2496–2506. doi: 10.1002/eji.201646347.

Carbon, S. *et al.* (2009) 'AmiGO: online access to ontology and annotation data', *Bioinformatics*. Oxford University Press, 25(2), pp. 288–289. doi: 10.1093/bioinformatics/btn615.

Chakraborty, P. *et al.* (2014) 'LIN28A Marks the Spermatogonial Progenitor Population and Regulates Its Cyclic Expansion', *STEM CELLS*, 32(4), pp. 860–873. doi: 10.1002/stem.1584.

Chen, E. Y. *et al.* (2013) 'Enrichr: interactive and collaborative HTML5 gene list enrichment analysis tool', *BMC Bioinformatics*, 14(1), p. 128. doi: 10.1186/1471-2105-14-128.

Chen, H. H. *et al.* (2014) 'DAZL limits pluripotency, differentiation, and apoptosis in developing primordial germ cells', *Stem Cell Reports*, 3(5), pp. 892–904. doi: 10.1016/j.stemcr.2014.09.003.

522 Chen, Y. *et al.* (2018) 'Single-cell RNA-seq uncovers dynamic processes and critical regulators
523 in mouse spermatogenesis', *Cell Research*, 28(9), pp. 879–896. doi: 10.1038/s41422-018-0074-
524 y.

525 Choi, I. *et al.* (2003) 'Identification and characterization of ADAM32 with testis-predominant gene
526 expression', *Gene*, 304(1–2), pp. 151–162. doi: 10.1016/S0378-1119(02)01202-7.

527 da Cruz, I. *et al.* (2016) 'Transcriptome analysis of highly purified mouse spermatogenic cell
528 populations: gene expression signatures switch from meiotic-to post-meiotic-related processes
529 at pachytene stage.', *BMC genomics*, 17(1), p. 294. doi: 10.1186/s12864-016-2618-1.

530 Engreitz, J. M. *et al.* (2013) 'The Xist lncRNA Exploits Three-Dimensional Genome Architecture
531 to Spread Across the X Chromosome', *Science*, 341(6147), pp. 1237973–1237973. doi:
532 10.1126/science.1237973.

533 Ernst, C. *et al.* (2019) 'Staged developmental mapping and X chromosome transcriptional
534 dynamics during mouse spermatogenesis', *Nature Communications*, 10, p. 1251. doi:
535 10.1038/s41467-019-09182-1.

536 Fallahi, M. *et al.* (2010) 'A Global Expression Switch Marks Pachytene Initiation during Mouse
537 Male Meiosis', *Genes*, 1(3), pp. 469–483. doi: 10.3390/genes1030469.

538 Feng, X. H., Lin, X. and Derynck, R. (2000) 'Smad2, Smad3 and Smad4 cooperate with Sp1 to
539 induce p15(Ink4B) transcription in response to TGF-beta.', *The EMBO journal*, 19(19), pp. 5178–
540 93. doi: 10.1093/emboj/19.19.5178.

541 Fernandez, P. C. (2003) 'Genomic targets of the human c-Myc protein', *Genes & Development*,
542 17(9), pp. 1115–1129. doi: 10.1101/gad.1067003.

543 Giorgetti, L. *et al.* (2016) 'Structural organization of the inactive X chromosome in the mouse.',
544 *Nature*, in press(7613), pp. 1–5. doi: 10.1038/nature18589.

545 Goldberg, E. *et al.* (2010) 'LDHC: The Ultimate Testis-Specific Gene', *Journal of Andrology*,
546 31(1), pp. 86–94. doi: 10.2164/jandrol.109.008367.

547 Goymer, P. (2005) 'Which mean do you mean?', *Nature genetics*, 6(December), pp. 2005–2005.
548 doi: 10.1080/00207398860170303.

549 Green, C. D. *et al.* (2018) 'A Comprehensive Roadmap of Murine Spermatogenesis Defined by
550 Single-Cell RNA-Seq', *Developmental Cell*, 46(5), p. 651–667.e10. doi:
551 10.1016/j.devcel.2018.07.025.

552 Griswold, M. D. (2016) 'Spermatogenesis: The Commitment to Meiosis', *Physiological Reviews*,
553 96(1), pp. 1–17. doi: 10.1152/physrev.00013.2015.

554 Grün, D. *et al.* (2015) 'Single-cell messenger RNA sequencing reveals rare intestinal cell types',
555 *Nature*. Nature Research, 525(7568), pp. 251–255. doi: 10.1038/nature14966.

556 Grün, D. *et al.* (2016) 'De Novo Prediction of Stem Cell Identity using Single-Cell Transcriptome
557 Data', *Cell Stem Cell*, 19(2), pp. 266–277. doi: 10.1016/j.stem.2016.05.010.

558 Grün, D., Kester, L. and van Oudenaarden, A. (2014) 'Validation of noise models for single-cell
559 transcriptomics.', *Nature methods*, 11(6), pp. 637–40. doi: 10.1038/nmeth.2930.

560 Grun, D. and van Oudenaarden, A. (2015) 'Design and Analysis of Single-Cell Sequencing
561 Experiments.', *Cell*, 163(4), pp. 799–810. doi: 10.1016/j.cell.2015.10.039.

562 Hart, P. E. *et al.* (1999) 'Testis-Specific Murine Centrin, Cetn1: Genomic Characterization and
563 Evidence for Retroposition of a Gene Encoding a Centrosome Protein', *Genomics*, 60(2), pp.
564 111–120. doi: 10.1006/geno.1999.5880.

565 Hasegawa, K. *et al.* (2015) 'SCML2 Establishes the Male Germline Epigenome through

566 Regulation of Histone H2A Ubiquitination', *Developmental Cell*, 32(5), pp. 574–588. doi:
567 10.1016/j.devcel.2015.01.014.

568 Hashimshony, T. *et al.* (2012) 'CEL-Seq: Single-Cell RNA-Seq by Multiplexed Linear
569 Amplification', *Cell Reports*. The Authors, 2(3), pp. 666–673. doi: 10.1016/j.celrep.2012.08.003.

570 Hashimshony, T. *et al.* (2016) 'CEL-Seq2: sensitive highly-multiplexed single-cell RNA-Seq',
571 *Genome Biology*. BioMed Central, 17(1), p. 77. doi: 10.1186/s13059-016-0938-8.

572 Hastie, T. and Stuetzle, W. (1989) 'Principal Curves', *Journal of the American Statistical*
573 *Association*. Taylor & Francis, 84(406), pp. 502–516. doi: 10.1080/01621459.1989.10478797.

574 van der Heijden, G. W. *et al.* (2007) 'Chromosome-wide nucleosome replacement and H3.3
575 incorporation during mammalian meiotic sex chromosome inactivation', *Nature Genetics*, 39(2),
576 pp. 251–258. doi: 10.1038/ng1949.

577 Henderson, S. A. (1963) 'Differential Ribonucleic Acid Synthesis Of X And Autosomes During
578 Meiosis.', *Nature*, 200, p. 1235. doi: 14089938.

579 Hermann, B. P. *et al.* (2018) 'The Mammalian Spermatogenesis Single-Cell Transcriptome, from
580 Spermatogonial Stem Cells to Spermatids', *Cell Reports*, 25(6), p. 1650–1667.e8. doi:
581 10.1016/j.celrep.2018.10.026.

582 Jan, S. Z. *et al.* (2017) 'Unraveling transcriptome dynamics in human spermatogenesis',
583 *Development*, p. dev.152413. doi: 10.1242/dev.152413.

584 Ji, Z. and Ji, H. (2016) 'TSCAN: Pseudo-time reconstruction and evaluation in single-cell RNA-
585 seq analysis', *Nucleic Acids Research*, 44(13), p. e117. doi: 10.1093/nar/gkw430.

586 Jiang, L. *et al.* (2017) 'RPL10L Is Required for Male Meiotic Division by Compensating for
587 RPL10 during Meiotic Sex Chromosome Inactivation in Mice', *Current Biology*, 27(10), p. 1498–
588 1505.e6. doi: 10.1016/j.cub.2017.04.017.

589 Jung, M. *et al.* (2018) 'Unified single-cell analysis of testis gene regulation and pathology in 5
590 mouse strains', *bioRxiv*, p. 393769. doi: 10.1101/393769.

591 Kasahara, T. *et al.* (2010) 'Genetic variation of melatonin productivity in laboratory mice under
592 domestication', *Proceedings of the National Academy of Sciences*, 107(14), pp. 6412–6417. doi:
593 10.1073/pnas.0914399107.

594 Khalil, A. M., Boyar, F. Z. and Driscoll, D. J. (2004) 'Dynamic histone modifications mark sex
595 chromosome inactivation and reactivation during mammalian spermatogenesis', *Proc Natl Acad*
596 *Sci U S A*, 101(47), pp. 16583–16587. doi: 10.1073/pnas.0406325101.

597 Khil, P. P. *et al.* (2004) 'The mouse X chromosome is enriched for sex-biased genes not subject
598 to selection by meiotic sex chromosome inactivation', *Nature Genetics*, 36(6), pp. 642–646. doi:
599 10.1038/ng1368.

600 Kim, B., Cooke, H. J. and Rhee, K. (2012) 'DAZL is essential for stress granule formation
601 implicated in germ cell survival upon heat stress', *Development*, 139, pp. 568–578. doi:
602 10.1242/dev.075846.

603 Koslowski, M. *et al.* (2006) 'The human X chromosome is enriched for germline genes
604 expressed in premeiotic germ cells of both sexes', *Human Molecular Genetics*, 15(15), pp.
605 2392–2399. doi: 10.1093/hmg/ddl163.

606 Kuleshov, M. V. *et al.* (2016) 'Enrichr: a comprehensive gene set enrichment analysis web
607 server 2016 update', *Nucleic acids research*, 44(W1), pp. W90–W97. doi: 10.1093/nar/gkw377.

608 Li, H. (2013) 'Aligning sequence reads, clone sequences and assembly contigs with BWA-MEM'.

609 Lukassen, S. *et al.* (2018) 'Characterization of germ cell differentiation in the male mouse

610 through single-cell RNA sequencing', *Scientific Reports*, 8(1), p. 6521. doi: 10.1038/s41598-018-
611 24725-0.

612 Luo, J., Megee, S. and Dobrinski, I. (2009) 'Asymmetric Distribution of UCH-L1 in
613 Spermatogonia Is Associated With Maintenance and Differentiation of Spermatogonial Stem
614 Cells', *Journal of Cellular Physiology*, 220(2), pp. 460–468. doi: 10.1002/jcp.21789.

615 Luo, M. *et al.* (2013) 'MEIOB exhibits single-stranded DNA-binding and exonuclease activities
616 and is essential for meiotic recombination.', *Nature communications*, 4(1), p. 2788. doi:
617 10.1038/ncomms3788.

618 Luo, M. *et al.* (2015) 'Polycomb protein SCML2 associates with USP7 and counteracts histone
619 H2A ubiquitination in the XY chromatin during male meiosis.', *PLoS genetics*. Edited by J. C.
620 Schimenti. Public Library of Science, 11(1), p. e1004954. doi: 10.1371/journal.pgen.1004954.

621 Mahadevaiah, S. K. *et al.* (2001) 'Recombinational DNA double-strand breaks in mice precede
622 synapsis.', *Nature genetics*. Nature Publishing Group, 27(3), pp. 271–6. doi: 10.1038/85830.

623 Mao, Q. *et al.* (2016) 'Principal Graph and Structure Learning Based on Reversed Graph
624 Embedding', *IEEE Transactions on Pattern Analysis and Machine Intelligence*, XX(X), pp. 1–1.
625 doi: 10.1109/TPAMI.2016.2635657.

626 Margolin, G. *et al.* (2014) 'Integrated transcriptome analysis of mouse spermatogenesis', *BMC*
627 *Genomics*, 15(1), p. 39. doi: 10.1186/1471-2164-15-39.

628 Matson, C. K. *et al.* (2010) 'The Mammalian Doublesex Homolog DMRT1 Is a Transcriptional
629 Gatekeeper that Controls the Mitosis versus Meiosis Decision in Male Germ Cells',
630 *Developmental Cell*, 19(4), pp. 612–624. doi: 10.1016/j.devcel.2010.09.010.

631 Matys, V. (2006) 'TRANSFAC(R) and its module TRANSCompel(R): transcriptional gene
632 regulation in eukaryotes', *Nucleic Acids Research*, 34(90001), pp. D108–D110. doi:
633 10.1093/nar/gkj143.

634 McKee, B. D. and Handel, M. A. (1993) 'Sex chromosomes, recombination, and chromatin
635 conformation', *Chromosoma*, 102(2), pp. 71–80. doi: 10.1007/BF00356023.

636 Meistrich, M. L. and Hess, R. A. (2013) 'Assessment of Spermatogenesis Through Staging of
637 Seminiferous Tubules', in Carrell, D. T. and Aston, K. I. (eds) *Spermatogenesis: Methods and*
638 *Protocols*. Totowa, NJ: Humana Press, pp. 299–307. doi: 10.1007/978-1-62703-038-0_27.

639 Mering, C. v. (2003) 'STRING: a database of predicted functional associations between
640 proteins', *Nucleic Acids Research*. Oxford University Press, 31(1), pp. 258–261. doi:
641 10.1093/nar/gkg034.

642 Monesi, V. (1965) 'Differential rate of ribonucleic acid synthesis in the autosomes and sex
643 chromosomes during male meiosis in the mouse', *Chromosoma*, 17(1), pp. 11–21. doi:
644 10.1007/BF00285153.

645 Muraro, M. J. *et al.* (2016) 'A Single-Cell Transcriptome Atlas of the Human Pancreas', *Cell*
646 *Systems*, 3(4), p. 385–394.e3. doi: 10.1016/j.cels.2016.09.002.

647 Nakata, H. *et al.* (2015) 'Quantitative analysis of the cellular composition in seminiferous tubules
648 in normal and genetically modified infertile mice.', *The journal of histochemistry and*
649 *cytochemistry : official journal of the Histochemistry Society*, 63(2), pp. 99–113. doi:
650 10.1369/0022155414562045.

651 Namekawa, S. H. *et al.* (2006) 'Post-meiotic Sex Chromatin in the Male Germline of Mice',
652 *Current Biology*, 16(7), pp. 660–667. doi: 10.1016/j.cub.2006.01.066.

653 Nguyen, T. B. *et al.* (2002) 'Characterization and Expression of Mammalian Cyclin B3, a
654 Prepachytene Meiotic Cyclin', *Journal of Biological Chemistry*, 277(44), pp. 41960–41969. doi:

10.1074/jbc.M203951200.

Nora, E. P. *et al.* (2012) 'Spatial partitioning of the regulatory landscape of the X-inactivation centre', *Nature*, 485(7398), pp. 381–385. doi: 10.1038/nature11049.

O'Shaughnessy, P. J., Morris, I. D. and Baker, P. J. (2008) 'Leydig cell re-generation and expression of cell signaling molecules in the germ cell-free testis', *Reproduction*, 135(6), pp. 851–858. doi: 10.1530/REP-07-0529.

Page, J. *et al.* (2012) 'Inactivation or non-reactivation: what accounts better for the silence of sex chromosomes during mammalian male meiosis?', *Chromosoma*, 121(3), pp. 307–326. doi: 10.1007/s00412-012-0364-y.

Petropoulos, S. *et al.* (2016) 'Single-Cell RNA-Seq Reveals Lineage and X Chromosome Dynamics in Human Preimplantation Embryos.', *Cell*, 165(4), pp. 1012–26. doi: 10.1016/j.cell.2016.03.023.

Portales-Casamar, E. *et al.* (2010) 'JASPAR 2010: the greatly expanded open-access database of transcription factor binding profiles.', *Nucleic acids research*. Oxford University Press, 38(Database issue), pp. D105-10. doi: 10.1093/nar/gkp950.

Primakoff, P. and Myles, D. G. (2000) 'The ADAM gene family: Surface proteins with adhesion and protease activity', *Trends in Genetics*, 16(2), pp. 83–87. doi: 10.1016/S0168-9525(99)01926-5.

Qiu, X. *et al.* (2017) 'Reversed graph embedding resolves complex single-cell trajectories.', *Nature methods*, 14(10), pp. 979–982. doi: 10.1038/nmeth.4402.

Raivo, K. (2013) *pheatmap: Pretty Heatmaps*.

Royo, H. *et al.* (2015) 'Silencing of X-Linked MicroRNAs by Meiotic Sex Chromosome Inactivation', *PLoS Genetics*, 11(10), pp. 1–15. doi: 10.1371/journal.pgen.1005461.

Russell, L. D. *et al.* (1993) *Histological and Histopathological Evaluation of the Testis*. doi: 10.1111/j.1365-2605.1993.tb01156.x.

Shin, Y.-H. *et al.* (2010) 'Hormad1 mutation disrupts synaptonemal complex formation, recombination, and chromosome segregation in mammalian meiosis.', *PLoS genetics*. Edited by R. S. Hawley, 6(11), p. e1001190. doi: 10.1371/journal.pgen.1001190.

Shiu, P. K. T. *et al.* (2001) 'Meiotic Silencing by Unpaired DNA', *Cell*, 107(7), pp. 905–916. doi: 10.1016/S0092-8674(01)00609-2.

Sun, F. *et al.* (2015) 'Nuclear localization of PRDM9 and its role in meiotic chromatin modifications and homologous synapsis.', *Chromosoma*, 124(3), pp. 397–415. doi: 10.1007/s00412-015-0511-3.

Supek, F. *et al.* (2011) 'Revigo summarizes and visualizes long lists of gene ontology terms', *PLoS ONE*. Edited by C. Gibas, 6(7), p. e21800. doi: 10.1371/journal.pone.0021800.

Szklarczyk, D. *et al.* (2017) 'The STRING database in 2017: quality-controlled protein–protein association networks, made broadly accessible', *Nucleic Acids Research*. Oxford University Press, 45(D1), pp. D362–D368. doi: 10.1093/nar/gkw937.

Tibshirani, R., Walther, G. and Hastie, T. (2001) 'Estimating the number of clusters in a data set via the gap statistic', *Journal of the Royal Statistical Society: Series B (Statistical Methodology)*, 63(2), pp. 411–423. doi: 10.1111/1467-9868.00293.

Turinetto, V. and Giachino, C. (2015) 'Multiple facets of histone variant H2AX: a DNA double-strand-break marker with several biological functions.', *Nucleic acids research*, 43(5), pp. 2489–98. doi: 10.1093/nar/gkv061.

699 Turner, J. M. A. *et al.* (2004) 'BRCA1, Histone H2AX Phosphorylation, and Male Meiotic Sex
700 Chromosome Inactivation', *Current Biology*, 14(23), pp. 2135–2142. doi:
701 10.1016/j.cub.2004.11.032.

702 Turner, J. M. A. (2015) 'Meiotic Silencing in Mammals.', *Annual review of genetics*, 49(1), pp.
703 395–412. doi: 10.1146/annurev-genet-112414-055145.

704 Vandesompele, J. *et al.* (2002) 'Accurate normalization of real-time quantitative RT-PCR data by
705 geometric averaging of multiple internal control genes', *Genome Biology*, 3(7), p.
706 research0034.1. doi: 10.1186/gb-2002-3-7-research0034.

707 Ventela, S. *et al.* (2000) 'Expression of green fluorescent protein under beta-actin promoter in
708 living spermatogenic cells of the mouse: stage-specific regulation by FSH', *International Journal*
709 *of Andrology*, 23(4), pp. 236–242. doi: 10.1046/j.1365-2605.2000.00237.x.

710 Vertesy, A. (2017) 'MarkdownReports: An R function library to create scientific figures and
711 markdown reports easily. Update v2.9.5'. doi: 10.5281/zenodo.1014353.

712 Wang, J. *et al.* (2017) 'NRF1 coordinates with DNA methylation to regulate spermatogenesis',
713 *The FASEB Journal*, 31(11), pp. 4959–4970. doi: 10.1096/fj.201700093R.

714 Xue, H. *et al.* (1999) 'HemT-3, an alternative transcript of mouse gene HemT specific to male
715 germ cells.', *Gene*, 240(1), pp. 193–9. doi: 10.1016/S0378-1119(99)00401-1.

716 Yoshinaga, K. *et al.* (1991) 'Role of c-kit in mouse spermatogenesis: identification of
717 spermatogonia as a specific site of c-kit expression and function.', *Development (Cambridge,*
718 *England)*, 113(2), pp. 689–99.

719 Zimmermann, C. *et al.* (2015) 'Research Resource: The Dynamic Transcriptional Profile of
720 Sertoli Cells During the Progression of Spermatogenesis', *Molecular Endocrinology*, 29(4), pp.
721 627–642. doi: 10.1210/me.2014-1356.

722

723

Figure legends

Fig.1: Single cell mRNA sequencing identifies five subtypes of *Dazl*-GFP+ germ cells, which correspond to subsequent stages of prophase-I.

a.) Experimental and analytic workflow.

b.) Transcriptome-wide k-medoids clustering identifies 5 clusters among 1274 high quality Dazl-GFP+ cells. Spearman correlation coefficients show homogenous and distinct clusters (cl. 1 & 5), while the three other stages are more heterogeneous.

c.) Cell-to-cell differences visualized on t-SNE map. Stages along the curve from left (1) to right (5) represent consecutive stages of prophase-I. Colors and numbers indicate clusters (as determined in panel B) and represent spermatogonial (1), (pre)leptotene I (2), zygotene (3), and pachytene (4,5) stages. Each dot represents a single cell.

d.) Expression of the selected marker genes. Negative and positive controls: No sorted cells express the Sertoli cell specific retinol binding protein 4 receptor (*Stra6*) or the Leydig cell specific anti-Mullerian hormone (*Amh*), but all cells express the sorting marker *Dazl*-GFP mRNA, validating sorting approach. Synaptonemal Complex Protein 3 (*Sycp3*) is a core component of the synaptonemal complex connecting homologous chromosomes in meiotic prophase. **Cl. 1** cells express spermatogonial markers *Lin28a* (progenitors) or *Kit* (differentiating spermatogonia). **Cl. 2** cells uniquely express the preleptotene marker *Stra8*, a key inducer of meiosis. **Cl. 3** cells the meiosis specific Cyclin B3 (*Ccnb3*) gene, which is located on the X chromosome, marking the last stage where sex chromosomes are expressed (zygotene). **Cl. 4** cells upregulate H2A histone family member X (*H2afx*), the histone variant associated with meiotic sex chromosome inactivation in early pachytene. **Cl. 5** cells specifically express many genes related to the function of spermatids. e.g.: lactate dehydrogenase C (*Ldhc*), testis-specific enzyme in anaerobic glycolysis, producing energy in motile sperm.

Fig. 2: Multiplexed trajectory reconstruction is consistent with established expression patterns and allows to explore gene expression at high temporal resolution.

a.) Pseudotemporal ordering is consistent across 3 different reconstruction methods (min. pairwise $r > 0.95$) and recapitulates the of stages (colors) defined earlier by marker genes. Each cell is a dot is a cell, ordered in 3 dimensions according to the pseudotime calculated by each algorithm (scaled 0-100) and colored as in Fig. 1.

b.) Consensus trajectory (color) is the average of the 3 methods and is represented on the tSNE map. Clusters are denoted by symbols.

c.) Three color single-molecule RNA FISH shows sequential expression of two consecutive prophase markers (*Stra8*, **Pl**: Preleptotene; *H2afx*, **P**: Pachytene) and the *Actb*, specifically upregulated in post-meiotic cells. Roman numeral: spermatogenic stage; **s1-16**: step 1-16 spermatids; * marks the lumen and dashed line marks the base of the tubule; scale bar: 10 µm.

d.) Relative expression of autosomes (grey) and sex chromosomes (X: red, Y: orange) throughout prophase-I. While autosomes are steadily expressed, sex chromosomes are sharply downregulated before pachytene. Rolling average of normalized chromosomal read counts are scaled to by the median expression along the trajectory. The inset shows

766 the raw transcript counts per cell as detected by sequencing, dropping before leptotene,
767 and sharply increasing in pachytene.

768 e.) Expression of later stage marker genes from (Fig. 1) and other key genes resolve
769 expression dynamics at a higher resolution. Early and late genes are separated in the top
770 and bottom panel for clarity. Gene expression is displayed as z-score normalized rolling
771 averages (window: 100). Temporal reconstruction precisely predicts expression timing.
772 *Lin28* peak is restricted to earliest *Dazl*+ spermatogonia, unlike *Kit*, and that the *Stra8*
773 slightly precedes *Prdm9*, as reported.

774 **Fig. 3: Systematic analysis of expression timing and co-expression patterns finds novel**
775 **co-expression patterns**

776 a.) K-means clustering of the 1077 highly expressed genes identifies specific peaking time
777 for each gene. Clustering was done on z-transformed moving averages of normalized
778 gene expression.

779 b.) Traces of all genes in class 3 show a clear expression peak between 400 and 600. The 3
780 sharpest peaking genes (by maximum z-score) are highlighted in color.

781 c.) Z-score normalized rolling average of raw transcript counts of all genes with a single,
782 sharp peak, ordered by their peaking times. Note that the number of unique genes
783 specific to the first (spermatogonia) and last (pachytene) cluster is inflated by nonspecific
784 genes expressed beyond the analyzed time window.

785 d.) Search for similar expression dynamics identified multiple genes (e.g: Ube2t, Hdac1,
786 Trim28) co-expressed with *H2afx*.

787 e.) *Gml* (*Hemt3*) vs *Gml2* (*Hemt1*) are the most stringently co-expressed genes with *H2afx*.

788 f.) Single-molecule RNA FISH shows the co-expression of *Gml2* and *H2afx* in Pachytene
789 (**P**) spermatocytes *in vivo.* Roman numeral: spermatogenic stage; **s1-16**: step 1-16
790 spermatids; * marks the lumen and dashed line marks the base of the tubule; scale bar:
791 10 µm. WGA staining omitted for clarity.

792 g.) Single-molecule RNA FISH with wheat germ agglutinin staining (WGA, in yellow). WGA
793 stains tubule boundaries and acrosomes, thus it allowed the staging of tubules in
794 combination with nuclear morphology. Two adjacent tubules of different stages. The
795 earliest pachytene cells are found in tubules of stage I-II, when pachytene cells just start
796 to upregulate pachytene specific genes. Scale Bar: 10 µm

797 **Fig. 4:. Meiotic entry is coupled to a downregulation of a tightly connected hub of**
798 **transcription factors, and coincides with metabolic and transcriptional silencing.**

799 a) Pairwise differential gene expression between spermatogonia (cl.1) and (pre)leptotene
800 (cl.2) cells shows 113, and 109 genes at least 4-fold enriched in either cluster, at
801 p.adj<$1e^{-6}$ (highlighted in red, Benjamini-Hochberg corrected). Selected gene names are
802 displayed. All significant genes are listed in (Table.S4).

803 b) Semantic similarity map shows key, stage specific biological processes. Significant GO-
804 terms within the 4-fold spermatogonia (**B**), and (pre)leptotene (**C**) enriched genes -as
805 identified in (A)- are grouped by similarity. Dot sizes correspond to the number of genes
806 associated, colours denote the -log10(False Discovery Rate). Representative GO-terms
807 with low FDR and high gene count are labeled.

c) See above.

d) Z-score normalized expression heatmap of at least 2-fold, significantly up- or downregulated genes in spermatogonia or (pre)leptotene cells. Cells in each cluster are ordered along the trajectory. Selected representative genes are labeled.

e) List of 8 transcription factors with significantly enriched (p.adj. < 0.001) binding sites within spermatogonia specific 2-fold enriched genes, using the TRANSFAC and JASPAR databases.

f) The identified transcription factors form a densely connected protein-protein interaction network as identified by STRING.

g) Rolling average (window: 100) normalized gene expression of the detected transcription factors along the trajectory. Dashed lines indicate approximate spermatogonial and (pre)leptotene boundaries along the trajectory.

Fig. 5: A wave of sex chromosomal gene activation precedes meiotic sex chromosome inactivation (MSCI)

a.) 34% of sex chromosomal genes are induced specifically before and silenced during MSCI. Genes are classified into 4 classes by k-means clustering of Z-score normalized rolling average gene expression profiles. Class 1 and 3 contains genes induced before and silenced by MSCI. Class 2 contains spermatogonia specific genes, while class 4 contains leptotene specific genes, and genes which are steadily expressed until MSCI.

b.) Both sex chromosomes show increasing relative expression before a rapid silencing that coincides with the induction of *h2afx* gene. Rolling average normalized expression values are divided by 100 for X, or by 10 for the Y chromosome for visualization. Dashed lines indicate the start and maximum of *h2afx* transcription, also marking the start and end of MSCI. Pearson correlation coefficients between the sex chromosomes' and *H2afx*'s expression during MSCI are denoted (X, Y, respectively). Grey dashed line indicates transcript counts per cell, as in Fig.2D.

c.) Gene expression of known post-transcriptional regulators of *H2afx*. As reported *Prkdc* is not expressed and *Atm* is only expressed earlier, during double strand break formation. The sole activator expressed during MSCI is *Atr*, and its' expression is unchanged after (pre)leptotene, suggesting that MSCI may not only be controlled at the post-transcriptional level.

d.) Average expression of all peaking genes (class 1&3) genes during MSCI (cl. 4) shows that a small set of genes is very highly expressed when meiotic silencing is already in progress.

e.) Individual traces of the highly expressed peaking genes (from **D**) shows a late and sharp silencing dynamics. *H2afx* expression (red), and MSCI boundaries (grey vertical lines) are displayed as a reference.

f.) Chromosomal location of the 27 sex chromosomal genes (all from chr. X) with an average expression above 1 in pachytene (cl.5).

g.) Highly expressed escapee genes. Average expression of sex chromosomal genes in pachytene II (cl.5) identifies a handful of escapee genes that are highly expressed after MSCI.

850 h.) The ampliconic gene *Mageb16* is the only MSCI-escapee gene, which is also described
851 to escape post-meiotic sex chromosome inactivation (PMSCI), and *Car5b* is the only
852 gene that is also described as an escapee in female X chromosome inactivation.

853 i.) *Slitrk2* is the only gene whose expression anti-correlated with the total expression from
854 the X-chromosome. While it is efficiently silenced before, it starts to be expressed during
855 MSCI and increases throughout pachytene.

856 j.) Single-molecule RNA FISH shows that *Slitrk2* escapes during late pachytene (right,
857 stage IX) and it maintains post-meiotic expression (left) spermatids *in vivo.* Roman
858 numeral: spermatogenic stage; **Se**: Sertoli cell; **L**: Leptotene; **P**: Pachytene; **s1-16**: step
859 1-16 spermatids; dashed line marks the base of the tubule; scale bar: 10 µm. WGA
860 staining omitted for clarity.

861 k.) Single-molecule RNA FISH with WGA staining (in yellow) shows continued *Slitrk2*
862 expression in spermatids, but it is not expressed in the earliest pachytene cells (cl. 4).
863 Scale Bar: 10 µm.

864

865 **Fig. 6: Genes in pachytene are induced in the same order as they are utilized in the**
866 **mature sperm.**

867 a.) Differential gene expression analysis identifies 635 genes that are at least 3-fold
868 upregulated in pachytene cells as compared to all other cells (p.adj < $1e^{-6}$, in red,
869 Benjamini-Hochberg corrected). Representative genes are labeled in black.

870 b.) Individual expression profiles of immediate genes show the step-like up regulation after
871 MSCI.

872 c.) The nuclear encoded mitochondrial gene, Cytochrome C Oxidase Subunit 8C (*Cox8c*) is
873 prime example of sharply upregulated genes.

874 d.) Gene expression profiles along the trajectory of the 635 genes were classified into 3
875 categories according to the shape and slope of increasing gene expression. K-means
876 clustering was performed on z-transformed moving average gene expression.

877 e.) Gradual genes all showed a slowly increasing gene expression in pachytene.

878 f.) The uncharacterized *Adam32* gene is suggested to be involved in sperm-egg fusion and
879 it shows the typical gradual accumulation of fertilization related genes.

880 g.) Significantly enriched GO-terms suggest markedly different function between the
881 immediate and gradual gene-sets (GO Biological Process and GO Cellular Component,
882 FDR<$1e^{-3}$). Immediate genes are enriched in energy and mobility related functions and
883 structures, while the gradually upregulated genes are enriched in fertilization related
884 functions and structures.

885 h.) Gradual- and immediate-class specific GO-terms map to different anatomical regions of
886 the sperm. Both unique and shared enriched GO-terms are analyzed, and informative
887 GO-terms are displayed. Gradual-class specific terms and corresponding anatomical
888 structures are in red. Immediate-class specific terms and structures are in green. Shared
889 terms and the related axoneme is indicated by the black arrow. The full list of GO-terms
890 is accessible in (Table S6).

i.) Single-molecule RNA FISH shows the upregulation of the fertility related *Adam32* after pachytene and its post-meiotic expression in spermatids *in vivo.* Roman numeral: spermatogenic stage; **B**: B spermatogonia; **P**: Pachytene spermatocyte; **s1-16**: step 1-16 spermatids; * marks the lumen and dashed line marks the base of the tubule; WGA staining for acrosomes is in yellow; scale bar: 10 µm.

Supplementary figure legends

Fig. S1. Filtering and quality control for clustering

- (**A**) Transcript count per cell shows a bimodal distribution. Low quality cells below 3000 transcripts are discarded (red). This results in 1274 high quality cells (green) with a median of 20488 reads.
- (**B**) Saturation determines the optimal cluster number in RaceID2. With increasing number of clusters, the Within Cluster Dispersion (WDC) decreases. When further increase of the number of clusters (**k**) yields a decrease (grey) that is within the estimated error interval (red) of the decrease, **k** is selected (5 in this case).
- (**C**) Gap Statistic did not yield a peak in single cell mRNA-seq datasets, therefore cannot be used to unambiguously determine the cluster number. Of not that it also saturates around 5, the cluster number determined by the saturation of within cluster dispersion.
- (**D**) The silhouette plots showed the average similarity of each cell to all cells in its own cluster, relative to other cells in the closest neighboring clusters. Positive values for most cells suggest that they are well represented within their own cluster.
- (**E**) High Jaccard index shows the high reproducibility of clusters across multiple bootstrapping rounds. The Jaccard index is calculated as the intersect over the union of cells in the same cluster across multiple bootstrapping rounds, pairwise. RaceID qualifies clusters reproducible above Jaccard index 60% (or 0.6).
- (**F**) Sequencing depth does not explain observed transcript count differences. Average over-sequencing per cell varies across individual cells a magnitude more than across clusters. Average oversequencing per cluster is lower in clusters with high transcript counts (cl1 & 5) as expected if the high read counts were explained by biology, and not by sequencing depth.

Fig. S2. Differences in transcriptome and clustering results are not explained by technical effects.

- (**A**) Distribution of cells across cell types, which were identified by k-medoids clustering.
- (**B-D**) Cells from all four libraries (**B**), all three animals (**C**), and cells prepared with either CEL-Seq1 or CEL-Seq2 primers (**D**) -- denoted by color, respectively -- contribute equally to all cell types (denoted by shapes), as shown on the t-SNE map.

928 • (**E-F**) Detected Gene and Transcript counts per cell detected both transiently decrease
929 from meiotic entry (cl.1→ cl.2) until a global transcriptional activation in pachytene
930 (cl.5).

931

932 **Fig. S3. Pseudotemporal ordering by three different algorithms**

933 • (**A**) Principal graph of cluster centers, and cell projections as reconstructed by Monocle 2
934 using DDRTree algorithm. Colors denote cell clusters as determined by RaceID,
935 colored by Monocle2.

936 • (**B**) Minimum spanning tree of cluster centers, as reconstructed by TSCAN (in black). Cells
937 were subsequently projected on this tree. Colors denote cell clusters identified by
938 TSCAN using a multivariate Gaussian mixture model in PCA space.

939 • (**C**) Reconstructed Principal Curve in t-SNE space and minimal cell projections, to the
940 curve. Colors denote cell clusters as determined by RaceID. Clustering results are not
941 used in this reconstruction, only provided for easier comparison.

942 • (**D**) Pairwise scatterplots and Pearson correlation coefficients across the 3 reconstruction
943 methods.

944 **Fig. S4. Filtering Peaking Genes by Quantile Ratio**

945 • (**A**) The ratio of the 100% and 95% quantiles of each gene's expression efficiently
946 distinguishes peaking genes (high maximal z-score) caused either by outlier
947 expression values, or by representative gene expression. While these genes both
948 have high z-score maxima (31 and 17 respectively), quantile ratio of two example
949 genes clearly separates outlier genes like *Prm1*. Log quantile ratio shown by dotted
950 lines for *Zfy2* (left) and *Prm1* (right).

951 • (**B-C**) Normalized transcript counts in single cells and rolling averages (in black, window:
952 50) of *Prm1* and *Zfy2*. Maximum z-scores of rolling averages are high in both cases,
953 however in the case of *Prm1*, this is clearly caused by one outlier cell with 1000
954 transcripts, thus it does not reflect a general change in expression.

955 • (**D**) Entropy quantifies the diversity of the transcriptome per cell and showed that
956 pachytene-II cells (cl.5) had transcriptome diversity even higher than spermatogonial
957 stem cells.

958

959 **Fig. S5. Expression patterns during and after MSCI in cluster 4 & 5**

960 • (**A**) Correlation network of gene expression plotted in PCA space. Spearman correlation
961 was calculated on the normalized expression patterns of sex chromosomal genes
962 along the trajectory within cluster 4 & 5. The blue arches represent high Spearman
963 correlation coefficients. All parameters were left as default in the *corrr* R-library. Most
964 genes are like *Ndufa1* (big cluster on the left), in that their normalized expression
965 (relative to the total transcript count per cell) decreases, while absolute transcript count
966 might stay at a similar level. Sporadically, escapee genes show particular expression

967 patterns, such as genes similar to *Ptchd1*, showing flat relative, increasing absolute
968 counts, or a strong increase such as *Slitrk2*.

969 • (**B**) The double peaking expression pattern of the multicopy *Rbmy* gene family.

970

971 **Fig. S6. Changes in molecular chaperones' expression coincides with major**
972 **transcriptional changes, (activation and silencing).**

973

974 • (**A**) Constitutively expressed (housekeeping) *Hsp90ab1* (90α-class b) and *Hspa8*
975 expression decreases upon meiotic entry, alongside with 3 chaperones involved in
976 protein import to mitochondria (*Hspd1*, *Hspe1*, and *Hspa4*)

977 • (**B**) From (pre)leptotene to zygotene a mixed set of chaperones is induced. The
978 constitutive *Hsp90b1* shows moderate induction (~20-30 mRNA/cell), while the
979 endoplasmic reticulum related, inducible *Hspa5* shows very strong upregulation (~70-
980 80 mRNA/cell). The signaling related small HSP member *Hspb11* shows a minor
981 (~5mRNA/cell), but distinct peak at meiotic entry.

982 • (**C**) The induced *Hsp90α* is known to be involved in cell cycle regulation, and it is strongly
983 induced upon meiotic entry, reaching ~150 transcripts per cell. Beside its role in stress
984 response, *Hsp90α* is also induced in response to the induction of excessive
985 translation. At the same time moderate to low induction of small HSPs *Hspb6* and
986 *Hspa4l*, and the *Hsp70* family member Hspa2, which is suggested to be involved in
987 spindle integrity.

988 • (D) Log10 scaled moving average gene expression of all displayed chaperones.
989 Importantly, immediate early genes (as defined in van den Brink et al 2017) are mostly
990 lowly expressed in the dataset, or specifically expressed at different stages (see also
991 at Data S5).

992

993 • (**E**) Expression of *Mid1 (Fxy)*, the only detected genes from the pseudoautosomal region
994 (PAR).

995

996

Supplementary table descriptions

Table S1: Differential gene expression: each cluster vs. all others

Differential gene expression analysis of each cluster as compared to all other clusters. Summary for each cluster (number of genes enriched), summary for each gene (arithmetic and geometric mean expression per cluster) and the enrichment statistic per gene, per comparison are provided.

Table S2: Differential gene expression: stepwise comparisons

Differential gene expression analysis of each cluster compared to the previous (in developmental order) cluster. Summary for each cluster (number of genes enriched), summary for each gene (arithmetic and geometric mean expression per cluster) and the enrichment statistic per gene, per comparison are provided.

Table S3: Changes of gene expression and function during meiotic entry.

TRANSFAC and JASPAR enrichment of transcription factors, binding to all at least 2-fold enriched genes; enrichment statistic per gene, per comparison; and the list of significantly enriched GO-terms in gene products of cluster 1 and 2 cells are provided.

Table S4: Changes of gene expression and function during meiotic sex chromosome inactivation

Characteristic silencing time and peak gene expression (rolling average) of sex chromosomal genes during MSCI; List of early-silenced genes and respective significantly enriched GO-terms; the same information for late-silenced genes; and finally, the list of sex chromosomal genes, which were used as a statistical background for the enrichment analysis.

Table S5: Changes of gene expression and function during pachytene activation

Cluster assignment of upregulated genes (k-means, k=3); list of and description of gene products for each cluster; and respective lists of enriched GO-terms are provided.

Supplementary dataset descriptions

Data S1 Transcriptome wide clustering as well as marker gene expression supports gradual, as opposed to switch-like differentiation of spermatogonia

A. *Dazl*+ spermatogonial transcriptome does not sub-cluster along *Kit* or *Lin28a*/*Sox13*/*Plzf* expression boundaries. Spearman or Pearson correlation based clustering of spermatogonia confirms overall transcriptional similarity observed in Fig. 1 regardless of the expression of Kit or the markers of undifferentiated spermatogonia. The cells that cluster apart are of lower quality, as defined by raw transcript counts.

B. Expression of reported markers of *Kit*-, undifferentiated spermatogonia. All spermatogonial cells exclusively express *Dmrt1*. 77% of spermatogonia express *Kit* (≥1 raw transcript), and only these cells also express Cyclins (*Ccnd1, Ccna2, Ccng1*). *Kit- Dazl*+ (and *Dmrt1*+) spermatogonia exclusively express a set of markers for undifferentiated spermatogonia: *Plzf* (or *Zbtb16*), *Sall4*, and *Sox13*. However, the expression of other markers for undifferentiated spermatogonia, such as: *Uchl1*, *Sox3*, *Stella* (*Dpp3*), or *Lin28a*), are not restricted to the Kit- population.

Data S3 Differential Gene Expression

Visual summary of differential gene expression analysis (Table S1-S2). Panels 1-5: comparison of cells in each cluster with all other cells. Panels 6-9: comparison of each cluster with the developmentally earlier cluster. Genes in red are significantly differentially expressed at $p < 1e^{-6}$ (Benjamini-Hochberg corrected).

Data S5 Stress.Genes.van.den.Brink.2017

Dissociation-induced genes (covering most early immediate genes) as defined in (Van Den Brink *et al.*, 2017), are mostly lowly expressed. Expressed "dissociation-induced genes" show varied dynamics along prophase-I and do not point to population of cells, which is particularly affected by the isolation procedure.

Supplementary online methods Vertesy et al

Mice strains, Organ Isolation and Dispersion

To separate germ cells from somatic cells, as well as to selectively sort germ cells from meiotic prophase-I, we used a mouse line expressing Dazl-GFP-V5 on a bacterial artificial chromosome (BAC). In this construct, the GFP sequence is integrated directly before the stop codon, and its expression is controlled by Dazl promoter and enhancer sequences (Chen *et al.*, 2014). *All mice were housed according to the Hubrecht Institute guidelines, which include access to food and water ad libitum. All animal experiments were carried out in compliance with standards for care and use of laboratory animals, with approval from the Dutch Animal Experiment Committee of The Royal Netherlands Academy of Arts and Sciences (KNAW). Mice were between 2 and 3 months old at time of sacrifice.*

In the first step, we isolated testicles from Dazl-GFP mice and chopped them into pieces. *Next, these tissue pieces were transferred to a 50 mL falcon tube and incubated in a collagenase type II (2 mg/mL Gibco, 17101015)/phosphate-buffered saline (PBS, Lonza, 17-516F) solution placed in a water bath set at 37 ºC for 1 hour to degrade the extracellular matrix and release cells from their niche. We used 10 mL collagenase solution per TA.* After this initial incubation, the tissue pieces were incubated in Trypsin at 37 degrees with gentle intermittent shaking for 8-10 min until the islets were dispersed into single cells. The dispersed tissue was washed briefly with cold PBS then filtered through a 25 µm sieve to remove debris and aggregates.

FACS Sorting

The Dazl-GFP mice allows us to select germ cells from spermatogonial up to pachytene spermatocyte stages, as Dazl expression in adult testes is restricted to germ cells of these stages. We used Propidium Iodide (PI) to exclude dead cells and VybrantViolet (cat. V35003) staining for DNA content to exclude haploid cells.

We incubated the cells with PI and VybrantViolet on ice before FACS-sorting, according to manufacturer's protocol. Cells were kept on ice until sorting. We used FACSJazz (BD biosciences) with the following configuration for all sorts Channel, Dye, Function: [488] 530/40, GFP, Dazl expression; [488] 585/29, PI, Live cells (PI negative); [405] 450/50,

1080 VybrantViolet, DNA content. Channel interpretation: [Excitation wavelength] Emission
1081 wavelength / Detection bandwidth.

1082 First, we selected single, live cells based on PI exclusion and scattering (P1 and P2 and
1083 P3). Next, we used GFP expression and VybrantViolet staining of Live Dazl-GFP
1084 positive single-cells. Finally, the selected cells were sorted into hard shell 384-well
1085 plates (Bio Rad, cat HSP3801) containing 200 nl of RT primers, dNTPs and synthetic
1086 mRNA Spike-Ins. To avoid evaporation, 5 µl of vapor-lock (QIAGEN, cat 981611) was
1087 added on top.

1088 After sorting, we spun down and froze the plates immediately. The plates were stored at
1089 -80˚C until processing. For details see (Van Den Brink *et al.*, 2017). For library
1090 preparation and sequencing we followed the SORT-seq protocol (Muraro *et al.*, 2016).

1091 Sorting experiments were done in biological triplicate and technical replicates. There
1092 were no relevant differences between replicates that would affect the conclusions. We
1093 both used CEL-seq1 and CEL-seq2 based primers. They showed differential sensitivity
1094 for a set of genes, which we effect we normalized out. See ***Analysis*** for consequences
1095 and normalization.

1096 Single-Cell mRNA library preparation

1097 We prepared cells into sequencing libraries by SORT-seq. For the detailed protocol,
1098 see: (Muraro *et al.*, 2016) and (Van Den Brink *et al.*, 2017). In brief, we used a 3-prime,
1099 poly-A based, UMI-corrected library construction protocol. SORT-seq is an improved
1100 and robotized version of the CEL-seq2 protocol designed for FACS sorted cells
1101 (Hashimshony *et al.*, 2016).

1102 Microscopy, single-molecule RNA fluorescence in situ hybridization
1103 (smFISH).

1104 For microscopy, testis isolated from 2-3 months old male wild type mouse were fixed in 4%
1105 RNAse free PFA at room temperature for 4 hours and cryopreserved by incubating overnight in
1106 30% glucose solution at 4C. Tissue was then cryomounted on OCT , frozen and sectioned into
1107 10µm thick slices. Tissue sections were then used for performing single-molecule RNA-FISH
1108 using the ViewRNA ISH Cell assay kit (Invitrogen: QVC0001). Tissue sections undergo a new
1109 fixation with 4% RNAse free PFA for 20 min at RT, permeabilization and protease treatment
1110 steps. Next, gene specific probe sets are hybridized (~20 oligos per gene), followed by

1111 sequential branched-DNA (bDNA) signal amplification, and finally individual mRNA molecules
1112 are visualized. The probes were designed to hybridize with the mRNAs of Stra8 (VB6-16903-
1113 VC), H2afx (VB1-3030165-VC), Actb (VB4-10432-VC), Gml2 (VB6-3223290-VC), Slirtk2 (VB6-
1114 3218124-VC), Adam32 (VB6-3221253-VC). Nuclei were stained by Hoechst, lectins were
1115 stained by Wheat Germ Agglutinin (WGA, molecular probes #W11261). Sections were imaged
1116 using a 63x objective on a PerkinElmer Ultraview VoX spinning disk microscope combined with
1117 a Leica SP8. Images were analyzed in ImageJ/FIJI.
1118

1119 Histology and staging of seminiferous tubules

1120 Seminiferous tubules a classified into 12 stages (I-XII) based the presence of different cell types
1121 (Russell *et al.*, 1993). Many cell types are indistinguishable by themselves under the microscope
1122 but can be inferred if the stage of the tubule is known, because only certain cell types are
1123 present at each tubule stage. Staging of tubules is based on nuclear and acrosomal morphology,
1124 as well as the position and presence of certain cells types (Meistrich and Hess, 2013). We
1125 staged tubules by fluorescence microscopy using a combination of fluorescent lectin conjugates
1126 and nuclear morphology (Nakata *et al.*, 2015). Stages are indicated by Roman numerals. Each
1127 image was recorded in 4 fluorescent channels, either DAPI + 3 smFISH probes, or DAPI + WGA
1128 + 2 smFISH probes. For clarity, DAPI + smFISH images are shown in the main figures, while
1129 WGA staining is not always shown.

1130 Data Analysis

1131 Alignment and Quantification

1132 Paired-end reads from Illumina sequencing were aligned to the mouse RefSeq
1133 transcriptome with BWA-MEM (Li, 2013). We trimmed low quality bases and discarded
1134 low quality and ambiguous alignments. For details on alignment, see (Grün *et al.*, 2015).
1135 After alignment, we removed UMI-duplicates from uniquely mapping reads. UMI-
1136 duplicates are reads from the same cell, same gene sharing the same unique molecular
1137 identifier revealing that they are were amplified from the same original mRNA molecule.
1138 Next, based on binomial statistics, we converted the number of observed UMI-s into
1139 transcript counts (Grün, Kester and van Oudenaarden, 2014).

Filtering

First, we selected cells with >2000 transcripts, yielding 1274 high quality cells. Next, we selected genes with at least 2 transcripts in at least 20 (out of 1274) cells. These cells had on average a median of 8079 transcripts from 1077 highly expressed genes.

Downsampling and normalization

Samples were normalized by taking the average of 10 downsampling rounds. Generally speaking, downsampling is better at keeping the statistical properties of the data, such as noise level, while normalization has no loss of information and therefore can be more sensitive. We combined these two approaches for an optimum solution. For downstream analysis, including k-medoids clustering, we used RaceID (Grün *et al.*, 2016) and custom scripts.

Normalization of libraries generated by CEL-seq1 and CEL-seq2 primers

As the SORT-seq protocol was designed during the time course of this study, we prepared libraries with two types of primers for reverse transcription. The original version is described in (Grün, Kester and van Oudenaarden, 2014), and it was based on CEL-seq1 (cs1) (Hashimshony *et al.*, 2012). Later, an optimized primer version was developed (Muraro *et al.*, 2016), which was based on the CEL-seq2 (cs2) protocol (Hashimshony *et al.*, 2016). We prepared 490 high quality (filtered) cells by cs1-, and 766 by cs2-primers.

To normalize the 2 protocols, first we calculated the average expression per gene over all index sorted plates per cs1 and cs2 batches. Next, we calculated the ratio of the batch averages, and normalized all genes to have the same average expression in both batches. After normalization we filtered highly expressed genes which are then used for clustering. Genes which had a more than 10-fold bias before normalization or were 4 times more often detected in either protocols were excluded from clustering. In Fig. S2 we show that cells from each batch contribute equally to all clusters regardless of primer design, biological replicate, or batch of library preparation.

Clustering and tSNE

For many steps of analysis, including k-medoids clustering of cells and tSNE projection, we used an in-house improved version of RaceID2 (Grün *et al.*, 2016). We implemented parallel computing in RaceID2 and extended its functionality to handle pseudotime related analysis and better accommodate multi-panel plotting. The code will be freely

available on https://github.com/vertesy/RaceID-v2.5-Multithreaded upon acceptance, with restriction to attribute the original author of RaceID upon use.

Establishing the number of clusters for k-medoids clustering

In RaceID, the optimal cluster number is determined as the saturation point of the Within Cluster Dispersion (WDC). By separating the data into more (thus smaller) clusters WDC decreases. When adding a new cluster yields a decrease that is no bigger than the estimated error interval of the decrease, k is selected. In this estimation, we repeatedly clustered cells into 1 to 10 preset clusters, and calculated WDC for each number of clusters. The optimal cluster number was estimated to be 5.

For comprehensiveness, we also calculated gap statistics (Tibshirani, Walther and Hastie, 2001). Gap statistic in single cell mRNA-seq datasets often does not yield a peak, therefore cannot determine the cluster number unambiguously. Nevertheless, it also saturates around 5, as estimated before

The silhouette plot shows the average similarity of each cell to all cells in its own cluster relative to all cells in the closest neighboring clusters. Positive values for most cells suggest that they are well represented within their own cluster. High Jaccard index shows high reproducibility of clusters across multiple bootstrapping rounds. The Jaccard index is calculated as the intersect over the union of cells in the same cluster across two bootstrapping rounds. RaceID qualifies clusters reproducible above Jaccard index 60%, while Jaccard indices in this study range 74-99%.

Differential Gene Expression

For differential gene expression analysis, we used RaceID2. The algorithm was specifically designed to model transcript count variability in single-cell data by a negative binomial noise model (Grün, Kester and van Oudenaarden, 2014), building on (Anders and Huber, 2010). P-values of significantly up or downregulated genes were calculated based on Poissonian statistics and corrected for multiple testing by the Benjamini-Hochberg method (Grün and van Oudenaarden, 2015).

We found that fold change as commonly calculated as the fraction of arithmetic mean (“average”) gene expression in compared cell types is not well suited for single cell data, as suggested previously (Bengtsson *et al.*, 2005).

Analysis based on arithmetic mean often identifies genes, which we consider false positives when looking at the raw expression data, in single cells. This is because arithmetic mean is a metric sensitive to outliers. It often indicates a big differences, which are not representative of the group of cells; in fact they are regularly caused by a few outlier cells with very high expression.

Median is commonly used as an outlier robust metric of the central tendency, it however loses sensitivity at low integer read counts, which is the typical range the for majority of the genes in single cell data. Furthermore, median becomes meaningless if near 50% of the cells have 0 expression (also known as zero-inflated data). Subtype specific genes with a narrow expression window are often overlooked by using median (e.g.: Zfy1 & 2).

Geometric mean is both robust against outliers and handles zero-inflated data, and it was found to be the appropriate metric for gene expression data that varies on the log-scale (Vandesompele *et al.*, 2002; Bengtsson *et al.*, 2005; Goymer, 2005). We therefore used the fold change of geometric means alongside the classical definition of fold change of arithmetic means, so that a gene must satisfy the same threshold for both metrics. This largely decreased our false positive detection, while maintaining similar sensitivity.

Expression patterns defining cluster boundaries

Groups of cells can be defined by either a unique expression of genes or by a combination of multiple non-unique expression patterns. We compared gene expression in each cluster to all other clusters to find uniquely expressed genes (TableS2), and we also compared gene expression in each cluster to the previous cluster (=developmental stage) to find gradual or stepwise changing genes (Table.S3).

GO-term enrichment

We found that GO-term enrichment on coding genes gives cleaner results, therefore we calculated GO-term enrichments using the STRING (v10.5) protein interaction database (Mering, 2003) everywhere, unless stated otherwise.

Functional enrichment and REViGO Analysis for spermatogonial and (pre)leptotene genes

We first performed pairwise differential gene expression between spermatogonial and (pre)leptotene clusters, then calculated GO-term enrichment on 4-fold enriched genes in either clusters. Next we analyzed the significantly enriched GO-terms (Biological Process, FDR < 0.05)

using REViGO (Supek *et al.*, 2011), with setting (similarity=0.9, semantic similarity measure: SimRel, associated values: -log10(FDR), GO term sizes: Mus musculus). REViGO first removes redundant (nested) GO terms, then calculates a 2 dimensional multidimensional scaling map based on semantic similarity of the terms. The full list of GO-terms is provided in (Table S3).

GO annotation defined gene sets

We first identified relevant GO-terms using EBI's QuickGo (Binns *et al.*, 2009) within the GO-term hierarchy. Next, we downloaded mouse gene annotations for each term, excluding negative annotation qualifiers using the AmiGO browser (Carbon *et al.*, 2009). We selected genes detected in our dataset and analyzed genes as described per analysis.

Pseudotemporal ordering of single cells

To draw a comprehensive picture of all genes changing expression at different times, we needed to reconstruct their developmental trajectory (Cannoodt, Saelens and Saeys, 2016). As we did not measure time, but infer, how long cells progressed in spermatogenesis, this procedure is called *pseudotemporal ordering*. We ordered cells according to gradual, transcriptome wide changes in gene expression by 3, distincts and established methods: Monocle 2 (Qiu *et al.*, 2017), TSCAN (Ji and Ji, 2016) and principal curve (Hastie and Stuetzle, 1989) as used in (Petropoulos *et al.*, 2016). The 3 methods are compared in their main features, dimensionality reduction, clustering, and trajectory modeling below.

Approach	Dimensionality Reduction	Clustering	Trajectory model	Ref
Monocle 2	DDRTree (discriminative dimensionality reduction via learning a tree)	k-medoids, provided by RaceID2	Principal Graph (a Principal Curve with branches allowed) learnt during dimensionality reduction by DDRTree.	(Qiu *et al.*, 2017)

TSCAN	PCA (Principal Component Analysis)	Multivariate gaussian mixture in PCA space	Minimum spanning tree of cluster centers	(Ji and Ji, 2016)
Principal Curve	tSNE (*t*-distributed stochastic neighbor embedding)	None	Principal Curve	(Hastie and Stuetzle, 1989)

Table: Comparison of the trajectory inference methods used.

Monocle 2

Monocle 2 identifies differentially expressed genes across clusters of cells (provided from RaceID2 in this case), then uses Discriminative Dimensionality Reduction with Trees (DDRTree) (Mao *et al.*, 2016), a Reversed Graph Embedding (RGE) algorithm to reconstruct a minimum spanning tree connecting cluster centroids, which is called principal tree. Cells then are projected to this principal tree, and their position along the backbone of the tree is counted as pseudo time. Monocle 2 uses an unsupervised inference method, where one does not need to feed the number of trajectories or paths, nor branching points. In fact multiple minor (<8% of the cells) side branches are detected by the algorithm, which all fall close to the main tree (Fig. S3).

TSCAN

In TSCAN, we provide the filtered normalized dataset. TSCAN uses PCA to reduce the dimensionality, which is followed by clustering by fitting a mixture of multivariate normal distributions using the Mclust package. The number of clusters here is determined by Bayesian information criterion, in our case it was 5. Next, TSCAN connects cluster centers with a minimum spanning tree, and finally it projects single cells on the tree, which is the cell order (Fig. S3 B).

Principal Curve

We fitted a principal curve (Hastie and Stuetzle, 1989), as in (Petropoulos *et al.*, 2016) to the two-dimensional t-SNE map (Fig. 1 A) of the cells in 100 iterations. The curve is initialized as a line segment; we use first principal component line. Next, each point of the curve is recalculated as a local average of all data points that project to this points using a spline smoothing with 4 degrees of freedom (smooth.spline function). In the next round new projections are calculated, etc. Already after 10 iterations the curve converged. The final curve was calculated after 100 iterations (Fig. S3 C).

Comparison and Consensus or Multiplex Pseudotime

Projection coordinates in all 3 approaches are scaled to [0,100] and pairwise Pearson correlation coefficients are calculated: TSCAN vs. Principal Curve: 0.956; TSCAN vs. Monocle: 0.973; Principal Curve vs. TSCAN: 0.956. Essentially all 3 algorithms captured the linear progress from spermatogonia to pachytene spermatocytes (Fig. 2 C). To further increase robustness, we calculated the consensus, or multiplex pseudotime as the average pseudotime for each cell in all three trajectories calculated by the different algorithms //Table.S3.

co-expression analysis

We calculated the Pearson correlation coefficient (r) over the normalized gene expression of pseudotime ordered cells.

Gml (Hemt3) and Gml2 (Hemt1)

Gml (*Hemt3*) and *Gml2* (*Hemt1*) is an interesting pair of genes, which are encoded on opposite strands, ~250 bases apart (ensembl mouse, GRCm38.p6, Chromosome 15: 74,806,933-74,812,856). While only Gml, but not Gml2 protein was shown to be expressed in spermatocytes in prophase (Xue *et al.*, 1999), the two transcripts show 89% sequence identity, as determined by blast alignment of the cDNAs. Sequencing reads show roughly equal and high read counts for both genes, suggesting that this readout is not due to sequencing errors (in such a case, one transcript would have 1-10% of the reads from the more abundant transcript).

Both transcripts are extremely well correlated with *H2afx* along pseudotime (r1 r2 =??), and accordingly, the Gml signal is correlated with *H2afx* signal in smFISH. However, because of the sequence similarity, it is not possible to resolve *Gml* and *Gml2* by

1304 smFISH (transcripts are tiled along with 20+ oligos), therefore smFISH gives a readout
1305 of these transcripts together.

1306 Early- and late-silenced genes on the sex chromosomes

1307 First, we selected all sex chromosomal genes that had a running median expression
1308 maximum above 1 during MSCI (pseudo time points 650-900) as defined by the *h2afx*
1309 expression ramp (Fig. 5B). To quantify the pace of gene expression changes, we
1310 defined the characteristic timescale of silencing (T_S) for each gene. T_S is defined in a
1311 way similarly to a substance's half-life: it is the time (pseudo time points) required for
1312 gene expression to drop to half of its maximal value, and it was corrected with an offset
1313 if the maxima did not coincide with beginning of MSCI. Without this correction, late
1314 activated genes, e.g. *Scml2,* would be mistakenly counted as an early-silenced gene. T_S
1315 was calculated on rolling average normalized gene expression with a window of 100.
1316 Finally, we ordered all genes according to their characteristic silencing timescale and
1317 divided the distribution into earlier and later half. We note that some reads mapped to a
1318 microRNA, Mir684-1. It is a multicopy gene across autosomes and the X chromosome.
1319 For this reason, and since CEL-seq is not suited to study microRNAs, we considered it a
1320 mapping artifact, therefore we excluded it from the analysis.

1321 GO-term enrichment was calculated on the interaction network of coding genes as
1322 described above. The statistical background for the enrichment were all coding genes on
1323 sex chromosomes present in the gene model used (mm10), (Grün, Kester and van
1324 Oudenaarden, 2014).

1325 Escapees

1326 As pachytene cells had ~9 fold more reads than zygotene, relative expression levels
1327 might not be indicative of leaky silencing, therefore we calculated expression of
1328 unnormalized transcript counts. The variation among single cells was counteracted by
1329 calculating a rolling average over the cells ordered along the trajectory.

1330 Classification gene expression patterns along the trajectory

1331 First, the normalized gene expression values of individual cells were ordered along the
1332 trajectory. Next, we calculated the rolling average expression with a window of 50 (or
1333 100 when indicated). To make genes with widely different expression levels comparable

regarding their activation or silencing time, we z-score transformed these values. Finally, this gene expression matrix was classified by k-mean clustering.

Transcriptome wide identification of time-specific or peak genes

As we extended our analysis to lowly expressed, we found many lowly expressed genes with specific expression times, such as *Zfy2* (Fig. S3 C). Expression peaks in ordered series can be identified by maximum z-score, however single outliers cause artifactual high z-scores (Fig. S3 B), but in this expression regime, one cannot filter on expression level. Therefore, we calculated the quantile-ratio, a metric that can robustly remove artifactual peaks. In this, we calculate the ratio of the 100% and 95% quantiles of each gene's expression. Genes only highly expressed in a few outlier cells have extremely high quantile ratio, and this metric efficiently distinguishes these genes from genes with true expression peaks (Fig. S3 A).

Analysis of Transcription Factor Binding sites

We found that meiotic entry from the spermatogonia towards preleptotene is characterized by global transcriptional silencing accompanied by the upregulation of defined set of genes. To find out which transcription factors driving these changes, we analyzed transcription factor binding sites enriched in the all genes that are at least 2-fold differentially expressed in cluster 2 vs 1, and vice versa. We used the online too *Enrichr* (Chen *et al.*, 2013; Kuleshov *et al.*, 2016), which searches across the TRANSFAC and JASPAR transcription factor binding profiles (Matys, 2006; Portales-Casamar *et al.*, 2010). *Enrichr* scans the −2000 and +500 vicinity of transcription start sites for transcription factor binding sites. The list of transcription factors with significantly enriched binding sites is then analyzed in the 2017 version of the amazing STRING database to identify functional and physical interactions, as well as GO-term enrichment (Mering, 2003; Szklarczyk *et al.*, 2017). We found that all upregulated genes are regulated by a tightly interconnected set of transcription factors.

Data And Software Availability

All analysis was performed in R-studio v1.0.136. For single cell analysis we used the StemID algorithm (Grün *et al.*, 2016) and custom scripts. Figures were generated by R packages pheatmap v1.0.8 (Raivo, 2013) and MarkdownReports v2.9.5 (Vertesy, 2017). Upon acceptance, the source code for analysis will be available "as-is" under GNU GPLv3 at https://github.com/vertesy/Spermatogenesis.Single-Cell. Sequencing data is deposited under accession number GSE114788 at GEO.

References for Supplementary Online Methods

Adams, S. R. *et al.* (2018) 'RNF8 and SCML2 cooperate to regulate ubiquitination and H3K27 acetylation for escape gene activation on the sex chromosomes', *PLoS Genetics*, 14(2). doi: 10.1371/journal.pgen.1007233.

Anders, S. and Huber, W. (2010) 'Differential expression analysis for sequence count data', *Genome biology*, 11(R106), pp. 1–12. doi: 10.1186/gb-2010-11-10-r106.

Anderson, E. L. *et al.* (2008) 'Stra8 and its inducer, retinoic acid, regulate meiotic initiation in both spermatogenesis and oogenesis in mice', *Proceedings of the National Academy of Sciences*, 105(39), pp. 14976–14980. doi: 10.1073/pnas.0807297105.

Aravin, A. a, Hannon, G. J. and Brennecke, J. (2007) 'The Piwi-piRNA pathway provides an adaptive defense in the transposon arms race.', *Science (New York, N.Y.)*, 318(5851), pp. 761–4. doi: 10.1126/science.1146484.

Baarends, W. M. *et al.* (2005) 'Silencing of unpaired chromatin and histone H2A ubiquitination in mammalian meiosis.', *Molecular and cellular biology*, 25(3), pp. 1041–53. doi: 10.1128/MCB.25.3.1041-1053.2005.

Bellani, M. A. *et al.* (2005) 'SPO11 is required for sex-body formation, and Spo11 heterozygosity rescues the prophase arrest of Atm-/- spermatocytes.', *Journal of cell science*, 118(Pt 15), pp. 3233–45. doi: 10.1242/jcs.02466.

Bengtsson, M. *et al.* (2005) 'Gene expression profiling in single cells from the pancreatic islets of Langerhans reveals lognormal distribution of mRNA levels', *Genome research*, pp. 1388–1392. doi: 10.1101/gr.3820805.4.

Berletch, J. B. *et al.* (2015) 'Escape from X inactivation varies in mouse tissues.', *PLoS genetics*. Edited by M. S. Bartolomei, 11(3), p. e1005079. doi: 10.1371/journal.pgen.1005079.

Bhattacharyya, T. *et al.* (2014) 'X Chromosome Control of Meiotic Chromosome Synapsis in Mouse Inter-Subspecific Hybrids', *PLoS Genetics*. Edited by B. A. Payseur, 10(2), p. e1004088. doi: 10.1371/journal.pgen.1004088.

Binns, D. *et al.* (2009) 'QuickGO: a web-based tool for Gene Ontology searching', *Bioinformatics*. Oxford University Press, 25(22), pp. 3045–3046. doi: 10.1093/bioinformatics/btp536.

Braydich-Stolle, L. *et al.* (2007) 'Role of Src family kinases and N-Myc in spermatogonial stem

cell proliferation', *Developmental Biology*, 304(1), pp. 34–45. doi: 10.1016/j.ydbio.2006.12.013.

Van Den Brink, S. C. *et al.* (2017) 'Single-cell sequencing reveals dissociation-induced gene expression in tissue subpopulations', *Nature Methods*, 14(10). doi: 10.1038/nmeth.4437.

Cannoodt, R., Saelens, W. and Saeys, Y. (2016) 'Computational methods for trajectory inference from single-cell transcriptomics', *European Journal of Immunology*, 46(11), pp. 2496–2506. doi: 10.1002/eji.201646347.

Carbon, S. *et al.* (2009) 'AmiGO: online access to ontology and annotation data', *Bioinformatics*. Oxford University Press, 25(2), pp. 288–289. doi: 10.1093/bioinformatics/btn615.

Chakraborty, P. *et al.* (2014) 'LIN28A Marks the Spermatogonial Progenitor Population and Regulates Its Cyclic Expansion', *STEM CELLS*, 32(4), pp. 860–873. doi: 10.1002/stem.1584.

Chen, E. Y. *et al.* (2013) 'Enrichr: interactive and collaborative HTML5 gene list enrichment analysis tool', *BMC Bioinformatics*, 14(1), p. 128. doi: 10.1186/1471-2105-14-128.

Chen, H. H. *et al.* (2014) 'DAZL limits pluripotency, differentiation, and apoptosis in developing primordial germ cells', *Stem Cell Reports*, 3(5), pp. 892–904. doi: 10.1016/j.stemcr.2014.09.003.

Chen, Y. *et al.* (2018) 'Single-cell RNA-seq uncovers dynamic processes and critical regulators in mouse spermatogenesis', *Cell Research*, 28(9), pp. 879–896. doi: 10.1038/s41422-018-0074-y.

Choi, I. *et al.* (2003) 'Identification and characterization of ADAM32 with testis-predominant gene expression', *Gene*, 304(1–2), pp. 151–162. doi: 10.1016/S0378-1119(02)01202-7.

da Cruz, I. *et al.* (2016) 'Transcriptome analysis of highly purified mouse spermatogenic cell populations: gene expression signatures switch from meiotic-to post-meiotic-related processes at pachytene stage.', *BMC genomics*, 17(1), p. 294. doi: 10.1186/s12864-016-2618-1.

Engreitz, J. M. *et al.* (2013) 'The Xist lncRNA Exploits Three-Dimensional Genome Architecture to Spread Across the X Chromosome', *Science*, 341(6147), pp. 1237973–1237973. doi: 10.1126/science.1237973.

Ernst, C. *et al.* (2019) 'Staged developmental mapping and X chromosome transcriptional dynamics during mouse spermatogenesis', *Nature Communications*, 10, p. 1251. doi: 10.1038/s41467-019-09182-1.

Fallahi, M. *et al.* (2010) 'A Global Expression Switch Marks Pachytene Initiation during Mouse Male Meiosis', *Genes*, 1(3), pp. 469–483. doi: 10.3390/genes1030469.

Feng, X. H., Lin, X. and Derynck, R. (2000) 'Smad2, Smad3 and Smad4 cooperate with Sp1 to induce p15(Ink4B) transcription in response to TGF-beta.', *The EMBO journal*, 19(19), pp. 5178–93. doi: 10.1093/emboj/19.19.5178.

Fernandez, P. C. (2003) 'Genomic targets of the human c-Myc protein', *Genes & Development*, 17(9), pp. 1115–1129. doi: 10.1101/gad.1067003.

Giorgetti, L. *et al.* (2016) 'Structural organization of the inactive X chromosome in the mouse.', *Nature*, in press(7613), pp. 1–5. doi: 10.1038/nature18589.

Goldberg, E. *et al.* (2010) 'LDHC: The Ultimate Testis-Specific Gene', *Journal of Andrology*, 31(1), pp. 86–94. doi: 10.2164/jandrol.109.008367.

Goymer, P. (2005) 'Which mean do you mean?', *Nature genetics*, 6(December), pp. 2005–2005. doi: 10.1080/00207398601703 03.

Green, C. D. *et al.* (2018) 'A Comprehensive Roadmap of Murine Spermatogenesis Defined by

Single-Cell RNA-Seq', *Developmental Cell*, 46(5), p. 651–667.e10. doi: 10.1016/j.devcel.2018.07.025.

Griswold, M. D. (2016) 'Spermatogenesis: The Commitment to Meiosis', *Physiological Reviews*, 96(1), pp. 1–17. doi: 10.1152/physrev.00013.2015.

Grün, D. *et al.* (2015) 'Single-cell messenger RNA sequencing reveals rare intestinal cell types', *Nature*. Nature Research, 525(7568), pp. 251–255. doi: 10.1038/nature14966.

Grün, D. *et al.* (2016) 'De Novo Prediction of Stem Cell Identity using Single-Cell Transcriptome Data', *Cell Stem Cell*, 19(2), pp. 266–277. doi: 10.1016/j.stem.2016.05.010.

Grün, D., Kester, L. and van Oudenaarden, A. (2014) 'Validation of noise models for single-cell transcriptomics.', *Nature methods*, 11(6), pp. 637–40. doi: 10.1038/nmeth.2930.

Grun, D. and van Oudenaarden, A. (2015) 'Design and Analysis of Single-Cell Sequencing Experiments.', *Cell*, 163(4), pp. 799–810. doi: 10.1016/j.cell.2015.10.039.

Hart, P. E. *et al.* (1999) 'Testis-Specific Murine Centrin, Cetn1: Genomic Characterization and Evidence for Retroposition of a Gene Encoding a Centrosome Protein', *Genomics*, 60(2), pp. 111–120. doi: 10.1006/geno.1999.5880.

Hasegawa, K. *et al.* (2015) 'SCML2 Establishes the Male Germline Epigenome through Regulation of Histone H2A Ubiquitination', *Developmental Cell*, 32(5), pp. 574–588. doi: 10.1016/j.devcel.2015.01.014.

Hashimshony, T. *et al.* (2012) 'CEL-Seq: Single-Cell RNA-Seq by Multiplexed Linear Amplification', *Cell Reports*. The Authors, 2(3), pp. 666–673. doi: 10.1016/j.celrep.2012.08.003.

Hashimshony, T. *et al.* (2016) 'CEL-Seq2: sensitive highly-multiplexed single-cell RNA-Seq', *Genome Biology*. BioMed Central, 17(1), p. 77. doi: 10.1186/s13059-016-0938-8.

Hastie, T. and Stuetzle, W. (1989) 'Principal Curves', *Journal of the American Statistical Association*. Taylor & Francis, 84(406), pp. 502–516. doi: 10.1080/01621459.1989.10478797.

van der Heijden, G. W. *et al.* (2007) 'Chromosome-wide nucleosome replacement and H3.3 incorporation during mammalian meiotic sex chromosome inactivation', *Nature Genetics*, 39(2), pp. 251–258. doi: 10.1038/ng1949.

Henderson, S. A. (1963) 'Differential Ribonucleic Acid Synthesis Of X And Autosomes During Meiosis.', *Nature*, 200, p. 1235. doi: 14089938.

Hermann, B. P. *et al.* (2018) 'The Mammalian Spermatogenesis Single-Cell Transcriptome, from Spermatogonial Stem Cells to Spermatids', *Cell Reports*, 25(6), p. 1650–1667.e8. doi: 10.1016/j.celrep.2018.10.026.

Jan, S. Z. *et al.* (2017) 'Unraveling transcriptome dynamics in human spermatogenesis', *Development*, p. dev.152413. doi: 10.1242/dev.152413.

Ji, Z. and Ji, H. (2016) 'TSCAN: Pseudo-time reconstruction and evaluation in single-cell RNA-seq analysis', *Nucleic Acids Research*, 44(13), p. e117. doi: 10.1093/nar/gkw430.

Jiang, L. *et al.* (2017) 'RPL10L Is Required for Male Meiotic Division by Compensating for RPL10 during Meiotic Sex Chromosome Inactivation in Mice', *Current Biology*, 27(10), p. 1498–1505.e6. doi: 10.1016/j.cub.2017.04.017.

Jung, M. *et al.* (2018) 'Unified single-cell analysis of testis gene regulation and pathology in 5 mouse strains', *bioRxiv*, p. 393769. doi: 10.1101/393769.

Kasahara, T. *et al.* (2010) 'Genetic variation of melatonin productivity in laboratory mice under

domestication', *Proceedings of the National Academy of Sciences*, 107(14), pp. 6412–6417. doi: 10.1073/pnas.0914399107.

Khalil, A. M., Boyar, F. Z. and Driscoll, D. J. (2004) 'Dynamic histone modifications mark sex chromosome inactivation and reactivation during mammalian spermatogenesis', *Proc Natl Acad Sci U S A*, 101(47), pp. 16583–16587. doi: 10.1073/pnas.0406325101.

Khil, P. P. *et al.* (2004) 'The mouse X chromosome is enriched for sex-biased genes not subject to selection by meiotic sex chromosome inactivation', *Nature Genetics*, 36(6), pp. 642–646. doi: 10.1038/ng1368.

Kim, B., Cooke, H. J. and Rhee, K. (2012) 'DAZL is essential for stress granule formation implicated in germ cell survival upon heat stress', *Development*, 139, pp. 568–578. doi: 10.1242/dev.075846.

Koslowski, M. *et al.* (2006) 'The human X chromosome is enriched for germline genes expressed in premeiotic germ cells of both sexes', *Human Molecular Genetics*, 15(15), pp. 2392–2399. doi: 10.1093/hmg/ddl163.

Kuleshov, M. V. *et al.* (2016) 'Enrichr: a comprehensive gene set enrichment analysis web server 2016 update', *Nucleic acids research*, 44(W1), pp. W90–W97. doi: 10.1093/nar/gkw377.

Li, H. (2013) 'Aligning sequence reads, clone sequences and assembly contigs with BWA-MEM'.

Lukassen, S. *et al.* (2018) 'Characterization of germ cell differentiation in the male mouse through single-cell RNA sequencing', *Scientific Reports*, 8(1), p. 6521. doi: 10.1038/s41598-018-24725-0.

Luo, J., Megee, S. and Dobrinski, I. (2009) 'Asymmetric Distribution of UCH-L1 in Spermatogonia Is Associated With Maintenance and Differentiation of Spermatogonial Stem Cells', *Journal of Cellular Physiology*, 220(2), pp. 460–468. doi: 10.1002/jcp.21789.

Luo, M. *et al.* (2013) 'MEIOB exhibits single-stranded DNA-binding and exonuclease activities and is essential for meiotic recombination.', *Nature communications*, 4(1), p. 2788. doi: 10.1038/ncomms3788.

Luo, M. *et al.* (2015) 'Polycomb protein SCML2 associates with USP7 and counteracts histone H2A ubiquitination in the XY chromatin during male meiosis.', *PLoS genetics*. Edited by J. C. Schimenti. Public Library of Science, 11(1), p. e1004954. doi: 10.1371/journal.pgen.1004954.

Mahadevaiah, S. K. *et al.* (2001) 'Recombinational DNA double-strand breaks in mice precede synapsis.', *Nature genetics*. Nature Publishing Group, 27(3), pp. 271–6. doi: 10.1038/85830.

Mao, Q. *et al.* (2016) 'Principal Graph and Structure Learning Based on Reversed Graph Embedding', *IEEE Transactions on Pattern Analysis and Machine Intelligence*, XX(X), pp. 1–1. doi: 10.1109/TPAMI.2016.2635657.

Margolin, G. *et al.* (2014) 'Integrated transcriptome analysis of mouse spermatogenesis', *BMC Genomics*, 15(1), p. 39. doi: 10.1186/1471-2164-15-39.

Matson, C. K. *et al.* (2010) 'The Mammalian Doublesex Homolog DMRT1 Is a Transcriptional Gatekeeper that Controls the Mitosis versus Meiosis Decision in Male Germ Cells', *Developmental Cell*, 19(4), pp. 612–624. doi: 10.1016/j.devcel.2010.09.010.

Matys, V. (2006) 'TRANSFAC(R) and its module TRANSCompel(R): transcriptional gene regulation in eukaryotes', *Nucleic Acids Research*, 34(90001), pp. D108–D110. doi: 10.1093/nar/gkj143.

McKee, B. D. and Handel, M. A. (1993) 'Sex chromosomes, recombination, and chromatin conformation', *Chromosoma*, 102(2), pp. 71–80. doi: 10.1007/BF00356023.

Meistrich, M. L. and Hess, R. A. (2013) ‘Assessment of Spermatogenesis Through Staging of Seminiferous Tubules’, in Carrell, D. T. and Aston, K. I. (eds) *Spermatogenesis: Methods and Protocols*. Totowa, NJ: Humana Press, pp. 299–307. doi: 10.1007/978-1-62703-038-0_27.

Mering, C. v. (2003) ‘STRING: a database of predicted functional associations between proteins’, *Nucleic Acids Research*. Oxford University Press, 31(1), pp. 258–261. doi: 10.1093/nar/gkg034.

Monesi, V. (1965) ‘Differential rate of ribonucleic acid synthesis in the autosomes and sex chromosomes during male meiosis in the mouse’, *Chromosoma*, 17(1), pp. 11–21. doi: 10.1007/BF00285153.

Muraro, M. J. *et al.* (2016) ‘A Single-Cell Transcriptome Atlas of the Human Pancreas’, *Cell Systems*, 3(4), p. 385–394.e3. doi: 10.1016/j.cels.2016.09.002.

Nakata, H. *et al.* (2015) ‘Quantitative analysis of the cellular composition in seminiferous tubules in normal and genetically modified infertile mice.’, *The journal of histochemistry and cytochemistry : official journal of the Histochemistry Society*, 63(2), pp. 99–113. doi: 10.1369/0022155414562045.

Namekawa, S. H. *et al.* (2006) ‘Post-meiotic Sex Chromatin in the Male Germline of Mice’, *Current Biology*, 16(7), pp. 660–667. doi: 10.1016/j.cub.2006.01.066.

Nguyen, T. B. *et al.* (2002) ‘Characterization and Expression of Mammalian Cyclin B3, a Prepachytene Meiotic Cyclin’, *Journal of Biological Chemistry*, 277(44), pp. 41960–41969. doi: 10.1074/jbc.M203951200.

Nora, E. P. *et al.* (2012) ‘Spatial partitioning of the regulatory landscape of the X-inactivation centre’, *Nature*, 485(7398), pp. 381–385. doi: 10.1038/nature11049.

O’Shaughnessy, P. J., Morris, I. D. and Baker, P. J. (2008) ‘Leydig cell re-generation and expression of cell signaling molecules in the germ cell-free testis’, *Reproduction*, 135(6), pp. 851–858. doi: 10.1530/REP-07-0529.

Page, J. *et al.* (2012) ‘Inactivation or non-reactivation: what accounts better for the silence of sex chromosomes during mammalian male meiosis?’, *Chromosoma*, 121(3), pp. 307–326. doi: 10.1007/s00412-012-0364-y.

Petropoulos, S. *et al.* (2016) ‘Single-Cell RNA-Seq Reveals Lineage and X Chromosome Dynamics in Human Preimplantation Embryos.’, *Cell*, 165(4), pp. 1012–26. doi: 10.1016/j.cell.2016.03.023.

Portales-Casamar, E. *et al.* (2010) ‘JASPAR 2010: the greatly expanded open-access database of transcription factor binding profiles.’, *Nucleic acids research*. Oxford University Press, 38(Database issue), pp. D105-10. doi: 10.1093/nar/gkp950.

Primakoff, P. and Myles, D. G. (2000) ‘The ADAM gene family: Surface proteins with adhesion and protease activity’, *Trends in Genetics*, 16(2), pp. 83–87. doi: 10.1016/S0168-9525(99)01926-5.

Qiu, X. *et al.* (2017) ‘Reversed graph embedding resolves complex single-cell trajectories.’, *Nature methods*, 14(10), pp. 979–982. doi: 10.1038/nmeth.4402.

Raivo, K. (2013) *pheatmap: Pretty Heatmaps*.

Royo, H. *et al.* (2015) ‘Silencing of X-Linked MicroRNAs by Meiotic Sex Chromosome Inactivation’, *PLoS Genetics*, 11(10), pp. 1–15. doi: 10.1371/journal.pgen.1005461.

Russell, L. D. *et al.* (1993) *Histological and Histopathological Evaluation of the Testis*. doi: 10.1111/j.1365-2605.1993.tb01156.x.

Shin, Y.-H. *et al.* (2010) 'Hormad1 mutation disrupts synaptonemal complex formation, recombination, and chromosome segregation in mammalian meiosis.', *PLoS genetics*. Edited by R. S. Hawley, 6(11), p. e1001190. doi: 10.1371/journal.pgen.1001190.

Shiu, P. K. T. *et al.* (2001) 'Meiotic Silencing by Unpaired DNA', *Cell*, 107(7), pp. 905–916. doi: 10.1016/S0092-8674(01)00609-2.

Sun, F. *et al.* (2015) 'Nuclear localization of PRDM9 and its role in meiotic chromatin modifications and homologous synapsis.', *Chromosoma*, 124(3), pp. 397–415. doi: 10.1007/s00412-015-0511-3.

Supek, F. *et al.* (2011) 'Revigo summarizes and visualizes long lists of gene ontology terms', *PLoS ONE*. Edited by C. Gibas, 6(7), p. e21800. doi: 10.1371/journal.pone.0021800.

Szklarczyk, D. *et al.* (2017) 'The STRING database in 2017: quality-controlled protein–protein association networks, made broadly accessible', *Nucleic Acids Research*. Oxford University Press, 45(D1), pp. D362–D368. doi: 10.1093/nar/gkw937.

Tibshirani, R., Walther, G. and Hastie, T. (2001) 'Estimating the number of clusters in a data set via the gap statistic', *Journal of the Royal Statistical Society: Series B (Statistical Methodology)*, 63(2), pp. 411–423. doi: 10.1111/1467-9868.00293.

Turinetto, V. and Giachino, C. (2015) 'Multiple facets of histone variant H2AX: a DNA double-strand-break marker with several biological functions.', *Nucleic acids research*, 43(5), pp. 2489–98. doi: 10.1093/nar/gkv061.

Turner, J. M. A. *et al.* (2004) 'BRCA1, Histone H2AX Phosphorylation, and Male Meiotic Sex Chromosome Inactivation', *Current Biology*, 14(23), pp. 2135–2142. doi: 10.1016/j.cub.2004.11.032.

Turner, J. M. A. (2015) 'Meiotic Silencing in Mammals.', *Annual review of genetics*, 49(1), pp. 395–412. doi: 10.1146/annurev-genet-112414-055145.

Vandesompele, J. *et al.* (2002) 'Accurate normalization of real-time quantitative RT-PCR data by geometric averaging of multiple internal control genes', *Genome Biology*, 3(7), p. research0034.1. doi: 10.1186/gb-2002-3-7-research0034.

Ventela, S. *et al.* (2000) 'Expression of green fluorescent protein under beta-actin promoter in living spermatogenic cells of the mouse: stage-specific regulation by FSH', *International Journal of Andrology*, 23(4), pp. 236–242. doi: 10.1046/j.1365-2605.2000.00237.x.

Vertesy, A. (2017) 'MarkdownReports: An R function library to create scientific figures and markdown reports easily. Update v2.9.5'. doi: 10.5281/zenodo.1014353.

Wang, J. *et al.* (2017) 'NRF1 coordinates with DNA methylation to regulate spermatogenesis', *The FASEB Journal*, 31(11), pp. 4959–4970. doi: 10.1096/fj.201700093R.

Xue, H. *et al.* (1999) 'HemT-3, an alternative transcript of mouse gene HemT specific to male germ cells.', *Gene*, 240(1), pp. 193–9. doi: 10.1016/S0378-1119(99)00401-1.

Yoshinaga, K. *et al.* (1991) 'Role of c-kit in mouse spermatogenesis: identification of spermatogonia as a specific site of c-kit expression and function.', *Development (Cambridge, England)*, 113(2), pp. 689–99.

Zimmermann, C. *et al.* (2015) 'Research Resource: The Dynamic Transcriptional Profile of Sertoli Cells During the Progression of Spermatogenesis', *Molecular Endocrinology*, 29(4), pp. 627–642. doi: 10.1210/me.2014-1356.

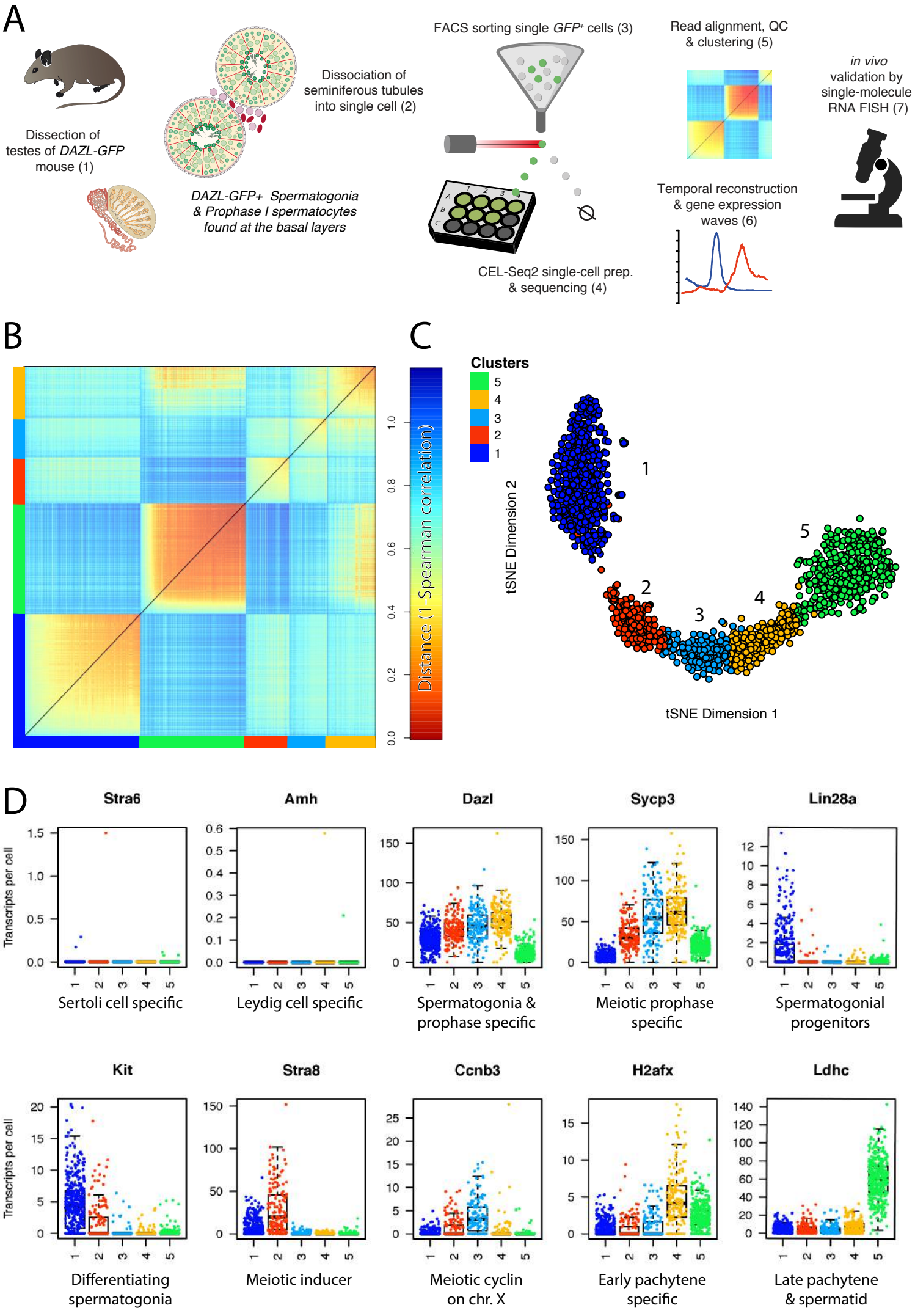
A
Dissection of testes of DAZL-GFP mouse (1)
Dissociation of seminiferous tubules into single cell (2)
DAZL-GFP+ Spermatogonia & Prophase I spermatocytes found at the basal layers
FACS sorting single GFP+ cells (3)
CEL-Seq2 single-cell prep. & sequencing (4)
Read alignment, QC & clustering (5)
Temporal reconstruction & gene expression waves (6)
in vivo validation by single-molecule RNA FISH (7)
B
Distance (1-Spearman correlation)
C
Clusters
5
4
3
2
1
tSNE Dimension 1
tSNE Dimension 2
D
Stra6
Amh
Dazl
Sycp3
Lin28a
Transcripts per cell
Sertoli cell specific
Leydig cell specific
Spermatogonia & prophase specific
Meiotic prophase specific
Spermatogonial progenitors
Kit
Stra8
Ccnb3
H2afx
Ldhc
Differentiating spermatogonia
Meiotic inducer
Meiotic cyclin on chr. X
Early pachytene specific
Late pachytene & spermatid

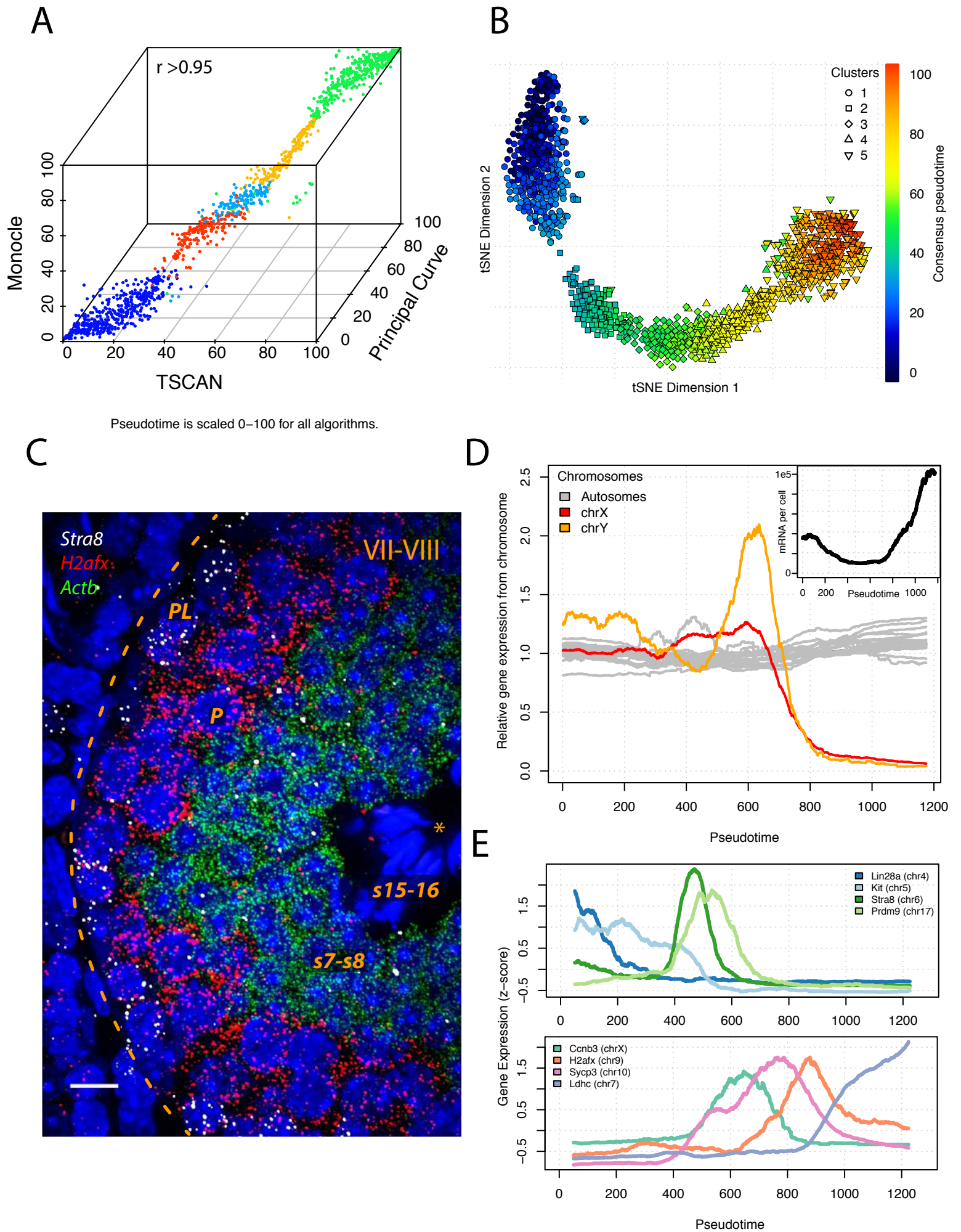
A
r >0.95
Monocle
TSCAN
Principal Curve
0
20
40
60
80
100
B
Clusters
1
2
3
4
5
tSNE Dimension 1
tSNE Dimension 2
Consensus pseudotime
Pseudotime is scaled 0–100 for all algorithms.
C
Stra8
H2afx
Actb
VII-VIII
PL
P
s15-16
s7-s8
D
Chromosomes
Autosomes
chrX
chrY
Relative gene expression from chromosome
mRNA per cell
1e5
Pseudotime
E
Lin28a (chr4)
Kit (chr5)
Stra8 (chr6)
Prdm9 (chr17)
Ccnb3 (chrX)
H2afx (chr9)
Sycp3 (chr10)
Ldhc (chr7)
Gene Expression (z−score)
Pseudotime

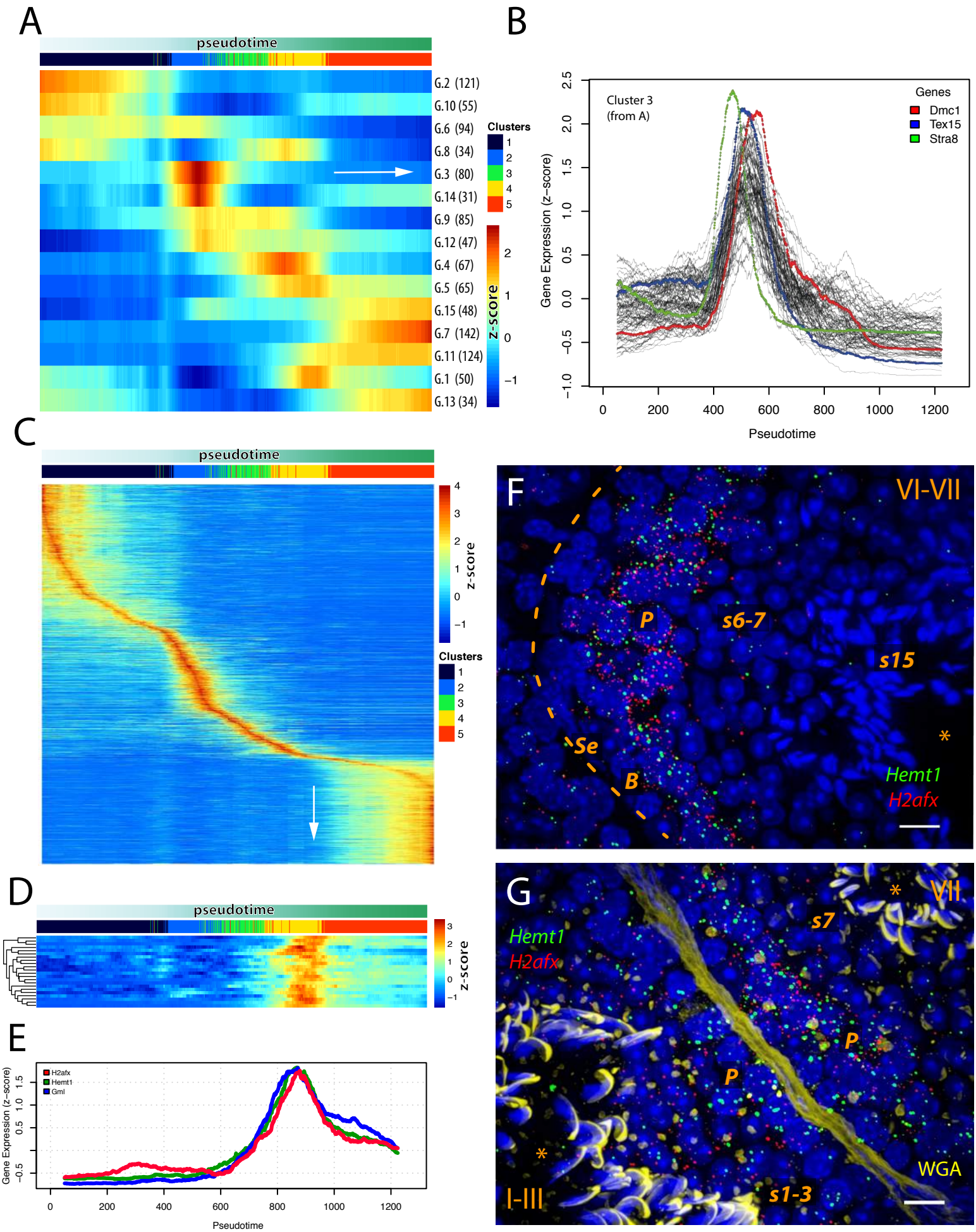
A
pseudotime
G.2 (121)
G.10 (55)
G.6 (94)
G.8 (34)
G.3 (80)
G.14 (31)
G.9 (85)
G.12 (47)
G.4 (67)
G.5 (65)
G.15 (48)
G.7 (142)
G.11 (124)
G.1 (50)
G.13 (34)
Clusters
1
2
3
4
5
z-score
2
1
0
−1
B
Cluster 3
(from A)
Genes
Dmc1
Tex15
Stra8
Gene Expression (z-score)
Pseudotime
C
pseudotime
z-score
Clusters
D
pseudotime
z-score
E
H2afx
Hemt1
Gml
Gene Expression (z-score)
Pseudotime
F
VI-VII
P
s6-7
s15
Se
B
Hemt1
H2afx
G
VII
s7
Hemt1
H2afx
P
P
WGA
I-III
s1-3

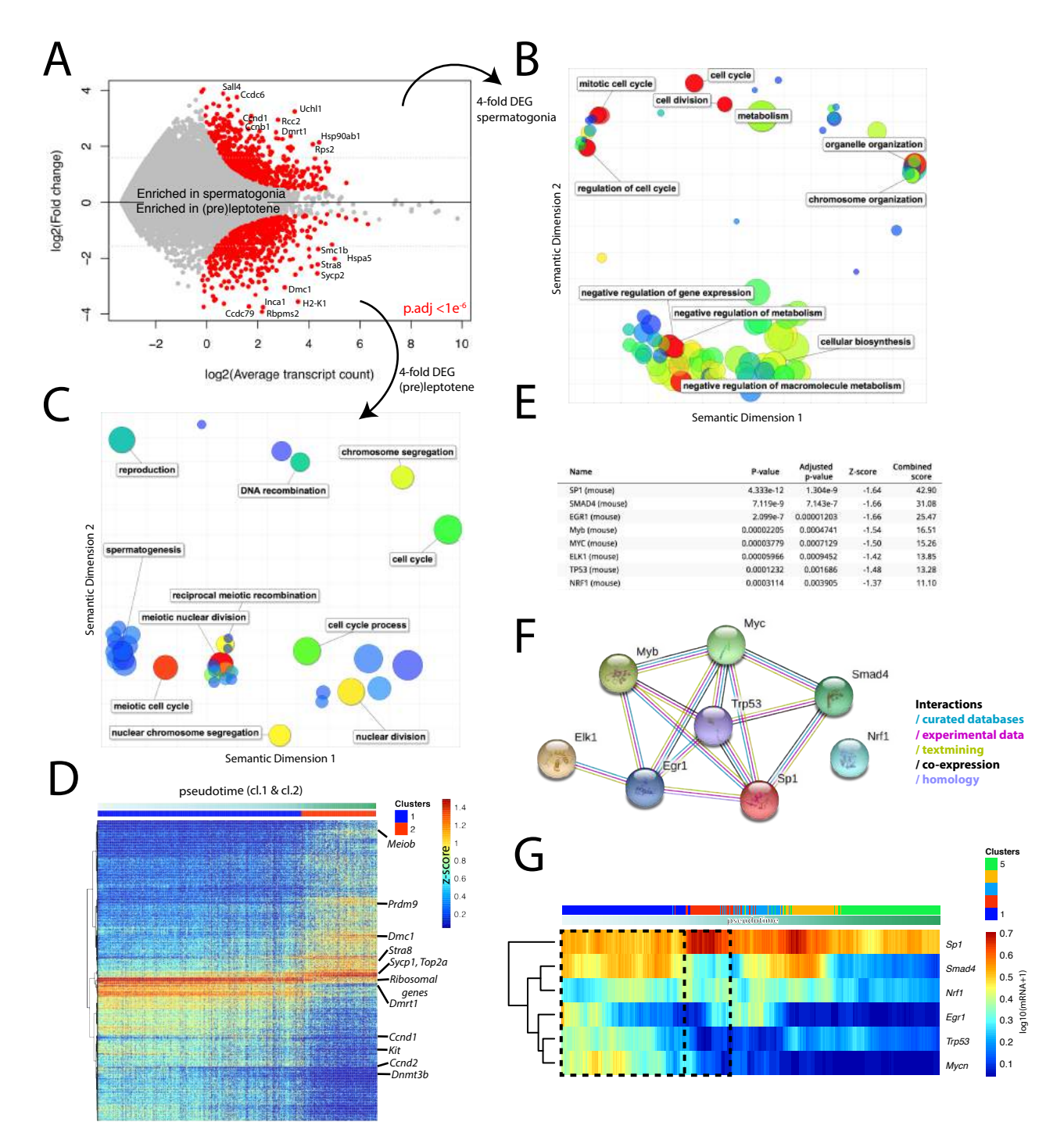

Name	P-value	Adjusted p-value	Z-score	Combined score
SP1 (mouse)	4.333e-12	1.304e-9	-1.64	42.90
SMAD4 (mouse)	7.119e-9	7.143e-7	-1.66	31.08
EGR1 (mouse)	2.099e-7	0.00001203	-1.66	25.47
Myb (mouse)	0.00002205	0.0004741	-1.54	16.51
MYC (mouse)	0.00003779	0.0007129	-1.50	15.26
ELK1 (mouse)	0.00005966	0.0009452	-1.42	13.85
TP53 (mouse)	0.0001232	0.001686	-1.48	13.28
NRF1 (mouse)	0.0003114	0.003905	-1.37	11.10

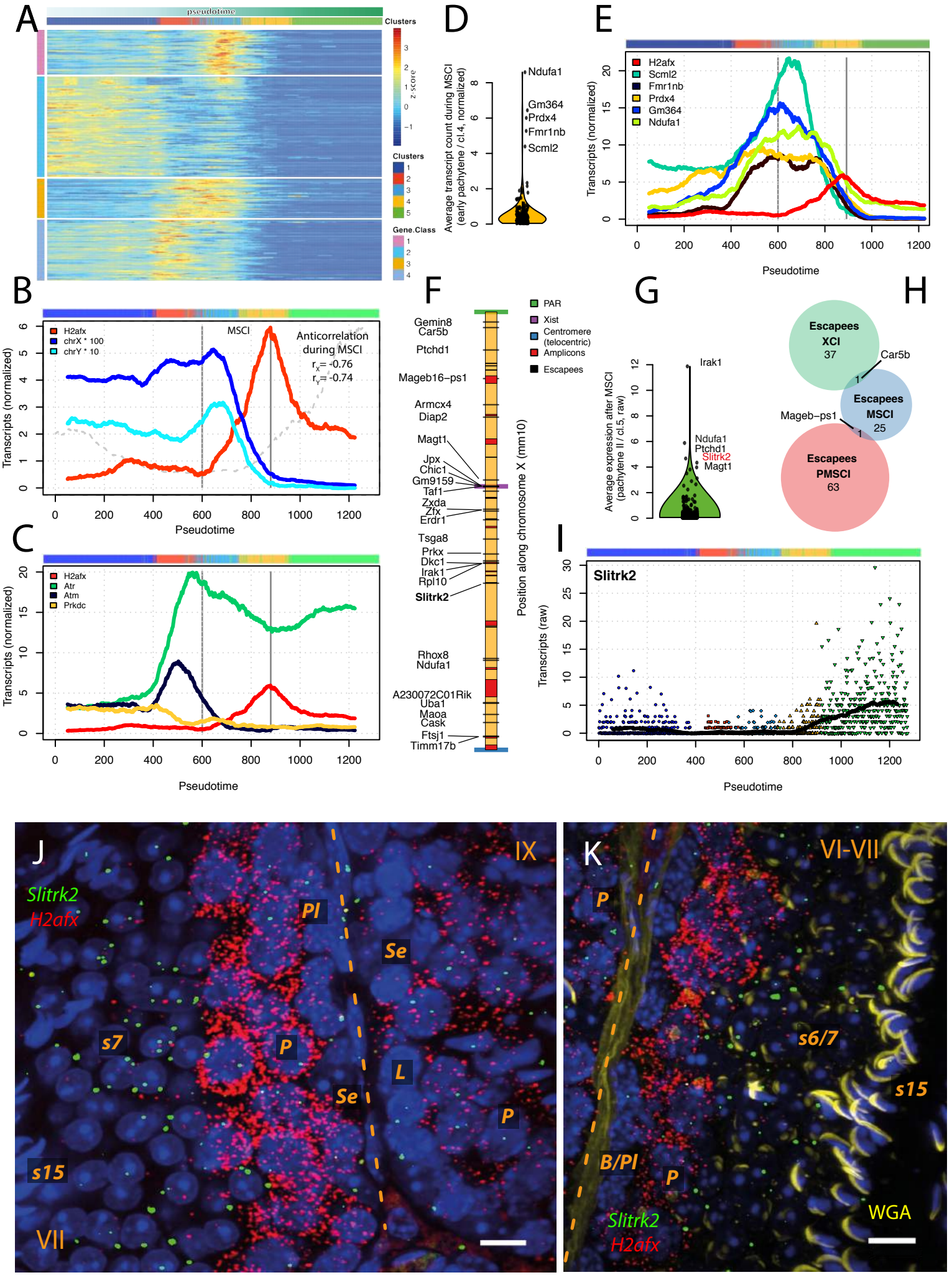
A
pseudotime
Clusters
z-score
Clusters
Gene.Class
B
H2afx
chrX * 100
chrY * 10
MSCI
Anticorrelation during MSCI
r_X = -0.76
r_Y = -0.74
Transcripts (normalized)
Pseudotime
C
H2afx
Atr
Atm
Prkdc
Transcripts (normalized)
Pseudotime
D
Average transcript count during MSCI (early pachytene / cl.4, normalized)
Ndufa1
Gm364
Prdx4
Fmr1nb
Scml2
E
H2afx
Scml2
Fmr1nb
Prdx4
Gm364
Ndufa1
Transcripts (normalized)
Pseudotime
F
PAR
Xist
Centromere (telocentric)
Amplicons
Escapees
Gemin8
Car5b
Ptchd1
Mageb16-ps1
Armcx4
Diap2
Magt1
Jpx
Chic1
Gm9159
Taf1
Zxda
Zfx
Erdr1
Tsga8
Prkx
Dkc1
Irak1
Rpl10
Slitrk2
Rhox8
Ndufa1
A230072C01Rik
Uba1
Maoa
Cask
Ftsj1
Timm17b
Position along chromosome X (mm10)
G
Average expression after MSCI (pachytene II / cl.5, raw)
Irak1
Ndufa1
Ptchd1
Slitrk2
Magt1
H
Escapees XCI 37
Escapees MSCI 25
Escapees PMSCI 63
Car5b
Mageb-ps1
I
Slitrk2
Transcripts (raw)
Pseudotime
J
Slitrk2
H2afx
IX
Pl
Se
s7
P
L
Se
P
s15
VII
K
VI-VII
P
s6/7
s15
B/Pl
P
Slitrk2
H2afx
WGA

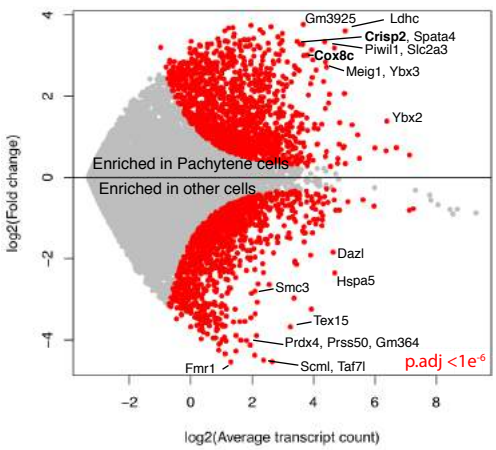

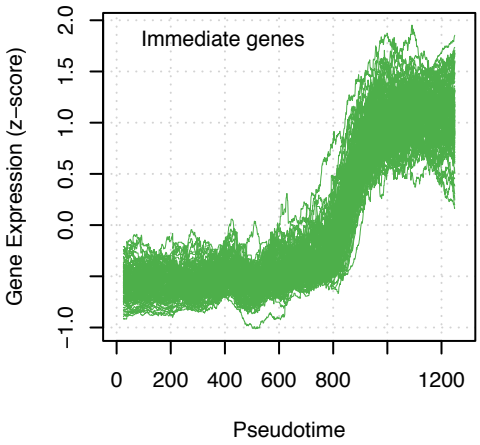

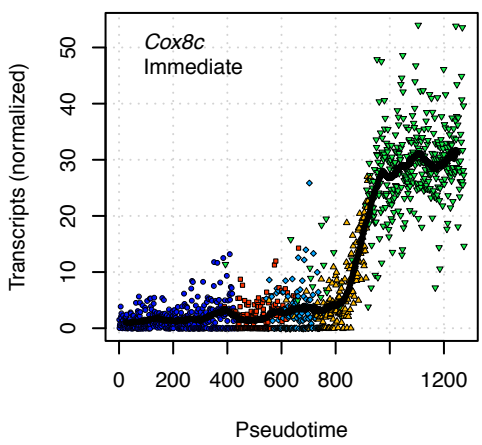

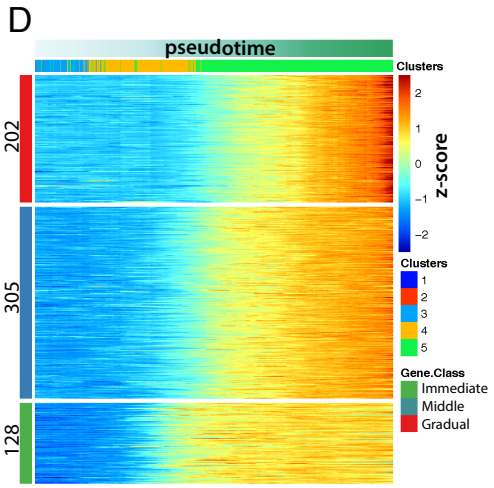

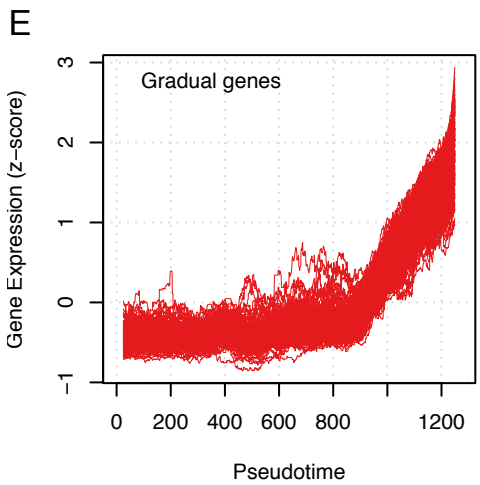

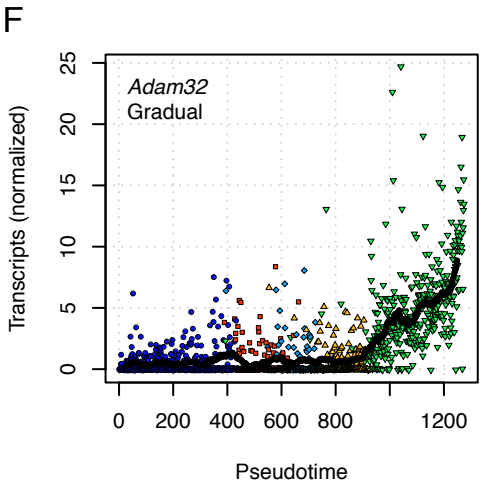

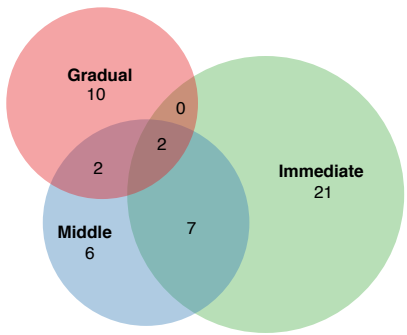
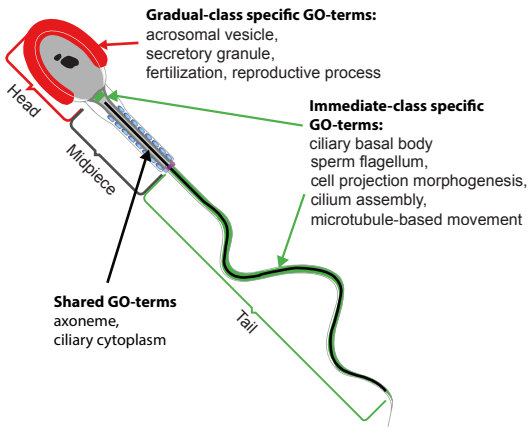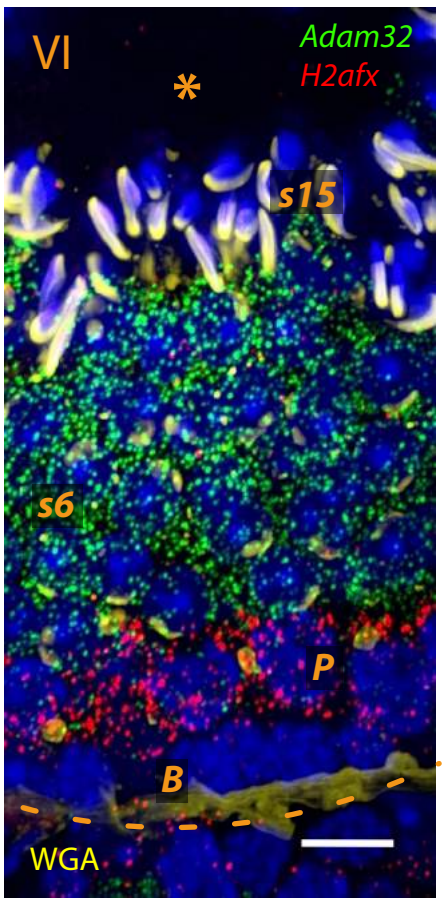
GO-terms Cellular Component and Biological Process, FDR < 0.001